MINERAL DISTRIBUTION SPATIALLY PATTERNS MESENCHYMAL STEM CELL BEHAVIOR ON MONOLITHIC BONE SCAFFOLDS

A Thesis

Presented to the Faculties of the Graduate School

of Cornell University

In Partial Fulfillment of the Requirements for the Degree of

Master of Science in Material Science and Engineering

Prepared by Hao Zhou

August 2019

ABSTRACT

The interfaces between soft tissue and bone at the ends of ligaments, tendons, and menisci, known as entheses, are characterized by their continuous apatitic mineral gradients. These interfacial tissues are essential to joint health, since they connect different tissues and mediate substantial changes in mechanical properties across the entheses. When damage occurs under extreme joint loading within an enthesis, repair of the enthesis is required to support growth locomotion and stability of joints. Implants are one possible repair route and fabricating implants that recapitulate the mineral gradient in native entheses can be challenging due to the complex, hierarchical structure of the interfacial tissue between bone and soft tissue. Tissue engineering provides a potential solution to repair damaged enthesis tissue by developing scaffolds that can be remodeled to mimic the extracellular matrix (ECM). Previously, we have demonstrated a 'top-down' method to create a monolithic bone scaffold with patterned mineral distribution at a scale around 40 microns and well-preserved native structure of trabecular bone. In this thesis, the cellular response to these scaffolds was studied. Mesenchymal stem cells (MSCs), which are the progenitor of most cells populations found in entheses, were seeded onto the scaffolds. Immunohistochemical (IHC) and histological stains were used to characterize their cellular behavior in regions of different mineral content. We found that MSCs in mineralized regions of the scaffold showed upregulated expression of osteogenic biomarkers, alkaline phosphatase (ALP) and osteocalcin (OCN) regardless of the presence of osteogenic biochemical cues in media. In contrast, MSCs in the demineralized regions of the scaffold showed downregulation of osteogenesis. In a chondrogenic biochemical environment, although osteogenesis was suppressed, MSCs in the mineralized regions of the scaffolds still showed

improved osteogenesis compared to those in the demineralized regions of the scaffolds. These results indicate that we can spatially control the osteogenesis of the MSCs using our bone scaffolds with spatially distributed mineral. Additionally, this study provides the framework to tissue engineer an entire enthesis with more biomimetic cellular complexity and better integration between soft and hard tissue.

BIOGRAPHICAL SKETCH

Hao Zhou was born on 1993 in Nantong, China. Growing up, he showed great interest in science fiction and technological creation. This enthusiasm led him to study science and engineering in different fields. He finished his Bachelor of Science Degree in Material Science and Engineering at University of Wisconsin, Madison in 2016. There, he joined Professor Ive Hermans's lab and studied metal oxide catalysts for oil fractioning. In the lab, he learnt how chemists and engineers can save energy through improving the selectivity of chemical reactions. He also finished an internship at Federal Mogul Powertrain with the valve seat and guide R&D group in Waupun, Wisconsin. He studied powder metallurgy and experienced the entire process from product design, testing to manufacture. In the group, he also developed a quick method to measure thermal conductivity of different metal alloys.

Hao started his Master of Science program in Material Science and Engineering department at Cornell University in 2017, co-advised by Professor Lara Estroff and Professor Lawrence Bonassar. This time, he set his sight on the field of tissue engineering. He contributed to the work in a newly developed method to fabricate a bio-mimetic scaffold with mineral gradients for enthesis tissue engineering. Followed by that, he characterized mesenchymal stem cell behaviors on the scaffold, which helped understand the cell-scaffold interactions and will contribute to the development of a tissue engineered meniscus. After graduation, Hao will continue his exploration in biomaterial and tissue engineering at University of Washington, Seattle for a PhD degree.

ACKNOWLEDGEMENTS

I sincerely thank everyone who helped me during the past 2 years in Cornell University. I specially thank Professor Lara Estroff and Professor Lawrence Bonassar, my advisors, for supporting me through this research. Their enthusiastic attitude towards science and positive personalities motivated me to overcome every challenge I met during research. I also thank Dr. Alexander Boys, Jongkil Kim, Dr. Joseph Druso for training me through most techniques I used to proceed this thesis work. I thank members of Bonassar lab and Estroff lab for giving me technical support in cell biology and material characterization. It is quite a fortune and pleasure to share two of my best years with you guys.

At last, I thank my parents for supporting me finishing my staying in Cornell University. I can never achieve all these without you.

CONTENTS

FIGURES

Chapter 1

Introduction and Background

1.1 Soft-Hard Tissue Interface

The interfacial structures between soft tissue and bone, known as entheses, showcase how biology integrates materials of different properties to support complex movement of the vertebrates[1,2]. There are mainly three types of entheses, in terms of ligamentous, tendinous and meniscal attachments. Based on the presence of the cellular types and extracellular matrix composition, these entheses can be generally divided in four zones: ligamentous zone, uncalcified fibrocartilage, calcified fibrocartilage and bone (Figure 1.1C)[3-5]. These zones are characterized by the presence of different cell phenotypes and the composition of extracellular matrix (ECM). The ligamentous zone consists of fibroblasts and aligned type I collage. The uncalcified fibrocartilage is defined by fibrochondrocytes, chondrocytes, unaligned type II and proteoglycans. The calcified fibrocartilage contains hypertrophic chondrocytes, type II and X collagen and hydroxyapatite (HAp). The bone contains osteoblast, osteoclasts, osteocytes, type I collagen and HAp. The morphology of the HAp crystals is unique in bone matrix. It is shaped as extremely thin platelet with 30-200 nm in length and width and 2-10 nm in thickness[6,7] (Figure 1.1A). The HAp mineral locates in the intrafibrillar interstices of the collagen fibril, with its c-axis parallelly aligned to the long axis of collagen fibril [8,9] (Figure 1.1B). These different ECM compositions and cellular populations contribute to the hierarchical, complex structures of the entheses tissue.

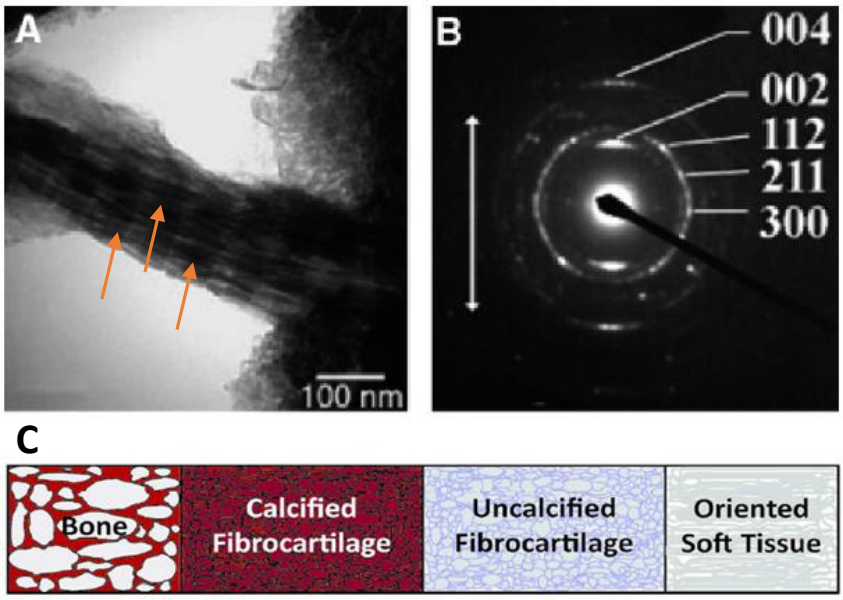

Figure 1.1 A) TEM brightfield image of mineralized collagen fiber in bone. Striations shown in arrows suggest the platelet-like morphology of the HAp crystal. B) Selected area electron diffraction of single collagen fiber from crushed equine bone. The arcing of (002) and (004) planes are the c-axis of the platelet, parallel to the orientation of the fibril as indicated by the white arrow. Other planes are in the a-b plane (reprinted from Ref. 8 (Materials Science and Engineering: R: Reports), with permission from Elsevier). C) Schematic of native enthesis structure.

1.2 Enthesopathies and Treatments to Meniscal Entheses

While entheses are precisely built, they can be injured under extreme joint load, fierce tension and torsion. Damage to entheses can lead to acute disability and degenerative joint disease such as enthesopathies. A common type of enthesopathy, for example anterior cruciate ligament (ACL) injury results in approximate 350,000 reconstruction surgeries annually in the US[10,11]. Patients with impaired entheses can eventually develop osteoarthritis (OA) even after operative interventions. Reportedly, 79% of those go through ACL reconstruction surgeries

develop OA and 20% of them re-injure their ACL postoperatively[12]. Therefore, a better understanding of how healthy entheses are structured and functions must be addressed to improve the performance of treatment to enthesopathies.

While the meniscus is commonly repaired through orthopedic surgeries, accounting for over 1 million annually per year in the US[13,14], re-establishing the meniscal enthesis is crucial to the success of these surgeries. The meniscal enthesis plays an essential role in fixing and stabilizing the meniscus while the meniscus itself functions as a cushion to absorb shock between femur and tibia and redistribute the joint load into radial orientations[5]. Some available treatments for meniscus injuries include meniscectomy, surgical repair and meniscal allograft. Total meniscectomy requires removal of the entire damaged meniscus, which in the long term can cause further damage to the cartilage and in fact accelerates joint damage[15]. Compared with total meniscectomy, partial meniscectomy is superior as it only removes the degraded meniscal part, which can preserve tissue of high importance to the biomechanical functioning of knee joints[16]. For specific tears in the meniscus, surgical repair can be done by suturing the tear back together. Such treatment has advantages of shortened recovery time and improved safety[13]. Due to these advantages, surgical repair is increasingly accepted by both patients and surgeons in the recent decade[15]. However, the success rate of meniscal repair can vary depending on the size and the location of the tear and the age of the patient[17]. Meniscal allograft transplantation is used when a total meniscal replacement is needed. It involves the fixation of a meniscal graft to the tibia with sutures. In a popular allografting method, the meniscal allograft is connected to suture thread via bone plugs attached at the horns[18,19]. A guide pin tunnel is then created beneath the tibia to allow the passage of the suture thread and anchor the bone plugs into the tibia (Figure 1.2A, B). The pitfall of this method is that drilling the tunnel can cause damage to the tibia and anterior cruciate

ligament (ACL)[18]. Moreover, the allograft may be dislocated and not an exact match to the original meniscus.

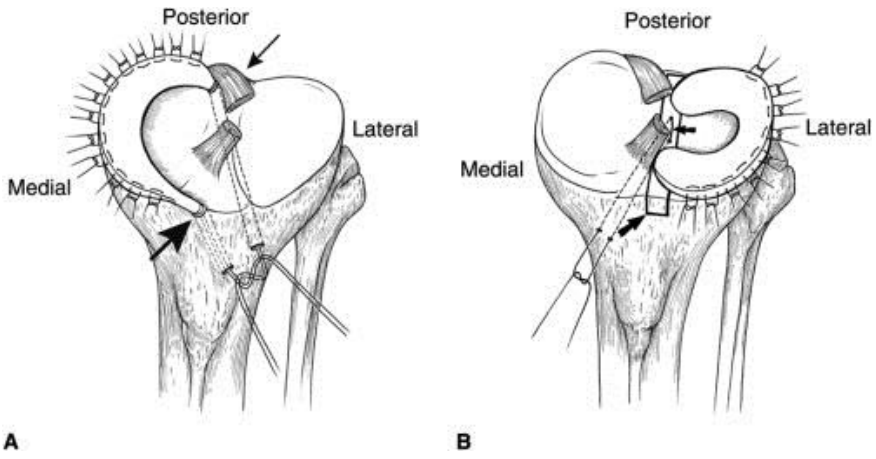

Figure 1.2 Meniscal allograft fixation via pin hole method. A) shows the fixation of the medial meniscus. B) shows the fixation of lateral meniscus (reprinted from Ref. 20 (Journal of the American Academy of Orthopaedic Surgeons), with permission from Wolters Kluwer Health, Inc).

1.3 Tissue Engineered (TE) Meniscus Model

A TE meniscus would provide an alternative solution to replace the damage meniscus and potentially restore its biomechanical functions. Previous work on TE meniscus focused on rebuilding the body of the meniscus[21,22]. Rarely were efforts put to construct meniscal entheses since the meniscal enthesis is different from other entheses. For example, the fibers of ligament and tendon align to the underlying bone whereas the meniscal fibers attach to the bone at an angle[23]. Therefore, the microstructure from meniscal soft tissue to bone is more challenging to recapitulate. A current *basic model* to study TE meniscal enthesis consists of a 3D printed type I collagen scaffold seeded with bovine fibrochondrocytes as meniscus and decellularized bovine

bone plugs as attachments[24] (Figure 1.3A, B). It has been demonstrated that in this model collagen infiltrated the porous bone matrix and establish a robust interface with the bone plug over a culture period of 4 weeks (Figure 1.3D). The elastic modulus and ultimate tensile strength of the construct, however, is several magnitudes below that of the native enthesis. Necking and failure usually occur at the bone-collagen interface, which suggests that the infiltration of collagen into the bone matrix is not enough to generate the interfacial strength matching the mechanical properties of the native enthesis.

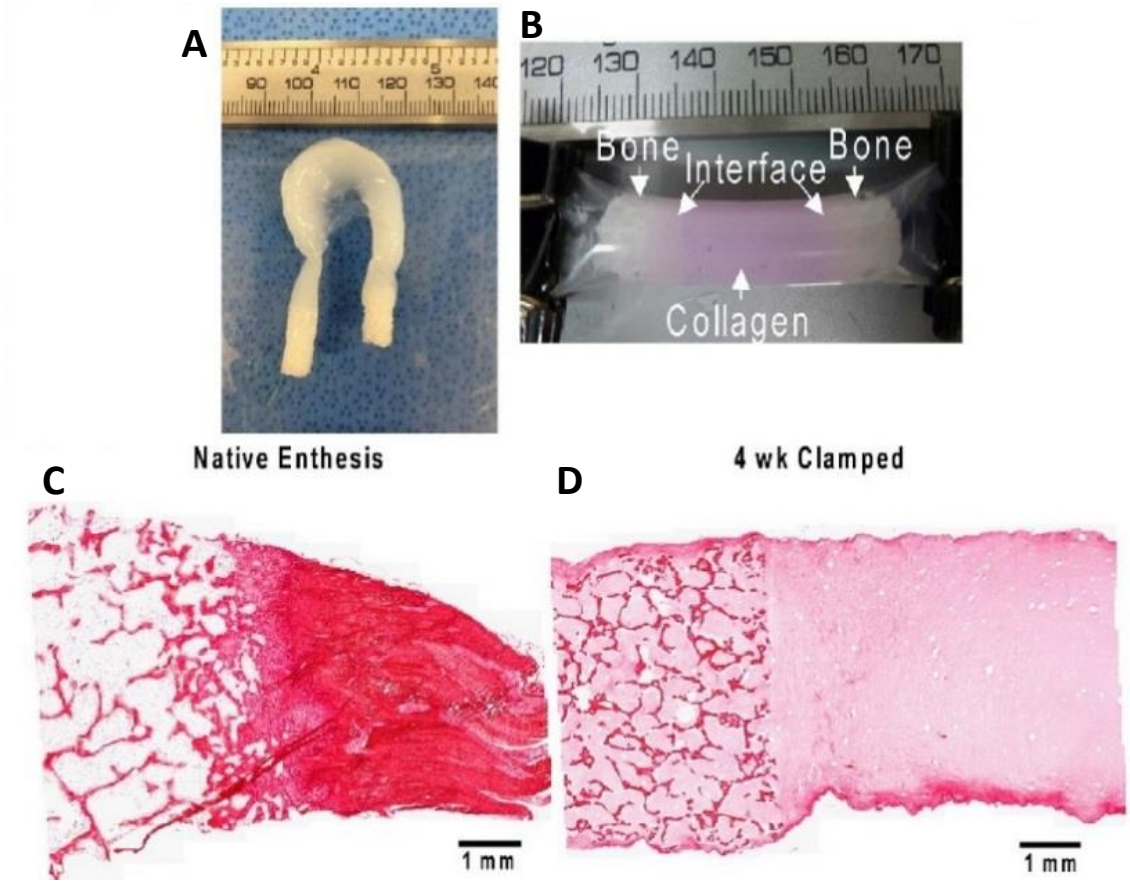

Figure 1.3 A) Tissue engineered meniscal enthesis with bovine fibrochondrocytes seeded collagen scaffold as meniscal body and bovine femur trabecular bone as hard tissue fixation. B) Simplified construct to study tissue engineered enthesis. C) Picrosirius red staining of enthesis interface from a native left caudal meniscal enthesis. D) Picrosirius red staining of tissue

engineered meniscal enthesis after 4 week clamped-culture (reprinted from Ref. 24 (Acta Biomater), with permission from Elsevier).

To reconstruct a tissue engineered meniscal enthesis, extracellular and cellular gradients are two important aspects to be considered. Within the extracellular matrix of the enthesis, there is a continuous gradient of HAp mineral distributed across the collagenous structure rather than an abrupt transition from mineralized to unmineralized tissue. This gradient was characterized by measuring the peak area ratio of mineral (phosphate peak) and nonmineral matrix (amide I peak) across a soft tissue-to-tibia insertion via Fourier-transform infrared spectroscopy (FTIR)[3] (Figure 1.4A). The mineral content across entheses can range from none in noncalcified tissue to 50 vol% or 65 wt% in bone[25]. Recapitulating this mineral gradient across the scaffold cannot only enhance the compositional biomimicry of the tissue-engineered enthesis but introduce gradual changes in material stiffness and strengthen the soft-hard material interface by minimizing the stress concentration as well[26].

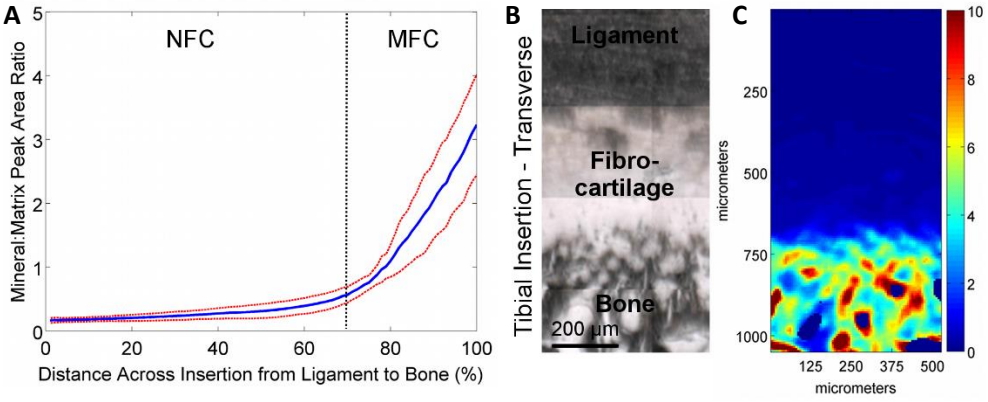

Figure 1.4 A) Mineral-matrix peak area ratio along the tibia insertion showed mineral gradient from ligament to bone. NFC=noncalcified fibrocartilage, MFC=calcified fibrocartilage. Blue

line =mean, Red line=standard deviation. B) Sample tibia insertion from neonatal bovine. C) Mapping mineral-matrix peak area ratio throughout the sample in B using FTIR microscopy. Red=high, Blue=low (reprinted from Ref. 3 (Materials Science and Engineering: R: Reports), with permission from Elsevier).

Since the bone plugs in the aforementioned *basic model* are acellular, the interface between bone plugs and collagen is only filled by fibrochondrocytes. This lack of cellular complexity across the interface can result in inferior mechanical properties at the soft-hard tissue interface, for example its ability to mediate tensile stress. Mesenchymal stem cells (MSCs) are a common therapeutic cell type that can be seeded onto scaffolds to reproduce the process of cellularization. MSCs are multipotent stromal cells found in bone marrow, adipose tissue and blood. They have the potential to differentiate into cell types including osteoblast, chondrocytes, myocytes and adipocytes based on their surrounding microenvironment[27-29]. In the bone marrow, MSCs play essential roles in the regeneration and maintenance of bone. Previous work of co-culturing MSCs in the bone scaffold with fibrochondrocytes in the collagen demonstrated improved integrity between the soft and hard material across the tissue-engineered meniscal enthesis[30]. Therefore, the introduction of cellular gradients is a promising strategy to improve the mechanical properties of TE entheses.

1.4 Decellularized Bone Matrix as Scaffolds

Prior to using bone plugs as the scaffolds to anchor the TE meniscus, synthetic scaffolds were usually developed to mimic the architecture of mineralized collagen in bone matrix. Olszta et al. reported the fabrication of HAp mineralized collagen scaffold (Cellagen®) using the

polymer-induced liquid-precursor (PILP) process[8]. The process was based on experiments showing anionic polypeptides (poly-aspartic acid) are able to capture and accumulate calcium ions in the fluidic amorphous phase from supersaturated solution, then form thermodynamically stable crystal phase of apatite. Electron diffraction on the mineralized collagen fibril showed the formation of platelet HAp with the (002) and (004) planes oriented to the long axis of the fibril (Figure 1.5C, D). This feature matches the morphology of HAp crystal presenting in native bone. However, the PILP process can only reach 30 wt% mineral content localizing at the outer region of the demineralized scaffolds, which is less than half of the mineral content in native bone[31]. Other bone-like materials such as mineralized peptide amphiphile nanofiber, show promising results in generating matching HAp crystal morphology and exhibit high biocompatibility *in vitro* and *in vivo*, but are not exact matches to the native bone due to limited amount of mineral deposition.

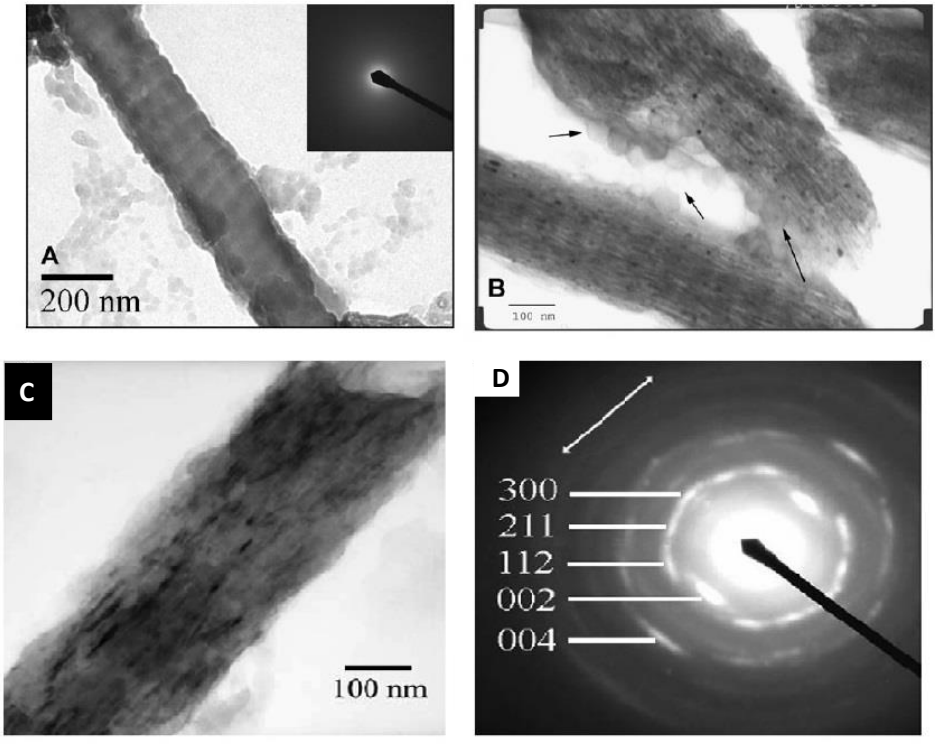

Figure 1.5 Collagen fibrils from Cellagen sponge during PILP mineralization process A) TEM of collagen fibril from Cellagen sponge at early stage of mineralization. Banding pattern indicates the entrenchment of amorphous calcium phosphate. Selected area electron diffraction shows no mineral formation within the fibril. B) TEM of collagen fibril from Cellagen sponge during mineralization. Striations parallel through the fibril suggests the formation of mineral. Arrows show the remaining PILP phase calcium phosphate. D) TEM bright-field image of single mineralized fibril via PILP process. Dark striations are platelets viewed edge on. E) Selected area electron diffraction pattern of E), (002) plane aligns to the long axis of the collagen which matches the crystal arrangement in bone (reprinted from Ref. 8 (Materials Science and Engineering: R: Reports), with permission from Elsevier).

The hunt for a scaffold shifts from synthesizing bone-like material to using decellularized bone, which maintains the architecture and composition of the ECM within the native bone. Native bone matrix contains bio-factors such as bone morphogenetic proteins (BMP) that can guide the osteogenic behavior of the attaching mesenchymal stem cells[32]. It can serve as an appropriate template for mineral deposition while maintaining the native mechanical properties of bone[33,34]. With proper decellularization process, the bio-factors and native ECM can be preserved, which will enhance the biocompatibility of the hard tissue in TE meniscal enthesis[35-37]. Trials of seeding MSCs in demineralized bone matrix (DMB) have been made where MSCs attached to the matrix and differentiated into cuboidal phenotype, an early sign of osteoblast lineage on day 14 of culture[38]. When dexamethasone, a corticosteroid drug commonly used to induce osteogenesis [39-40], was removed from the osteogenic media, the DMB matrix still

exhibited osteogenesis-inducing characteristic and resulted in partial osteogenic differentiation of MSCs.

1.5 Effect of Mineral Gradient on Stem Cell Differentiation

The relationship between mineral content of a scaffold and MSC behavior has been well studied as well. Dormer et al. proposed a PLGA-HAp microsphere-based scaffold prepared by emulsion method[41].The composition of the scaffolds ranged from 0 wt% to 20 wt% HAp. After human bone marrow stem cells were seeded, the 20 wt% HAp group exhibited the most Runx2 expression and fastest rate of ALP activity peak in week 1. Runx2 is a gene related to osteoblast lineage and ALP is an enzyme which sequesters organophosphate to produce HAp. These results suggested that the higher mineral content directed MSCs towards a more osteogenic differentiation pathway. In some other experiments including a comparison between mineralized and non-mineralized collagen-GAG scaffold, series of chitosan-HAp composite scaffolds with mineral content ranging from 0 to 50 wt%, an *in vivo* study of 10 and 30 wt% HAp-loaded chitosan-silk fibroin scaffold on nude mice, similar relationships between mineral content and MSC osteogenesis were observed[42-44].

Apart from inducing osteogenic behavior of MSCs, HAp was found to stimulate MSC differentiation towards chondrogenic lineages as well. Wang et al. have shown the biphasic correlation between HAp and chondrogenesis of ASCs[45]. For instance, in a chondrogenic biochemical environment, small amount of the HAp in a hyaluronic acid scaffold promoted the production of collagen and glycosaminoglycan by the ASCs. Increasing mineral content led to hypertrophic differentiation and upregulated expression of collagen X, Runx2, ALP and higher

tendency towards osteogenic differentiation. These results indicate the potential of applying HAp to establish the cell complexity from calcified to noncalcified cartilage region of TE enthesis.

While experiments with different HAp content in individual scaffolds provided useful information to pattern osteogenesis and chondrogenesis by MSCs, rebuilding the soft-hard tissue interface will require a continuous gradient of HAp content in a single scaffold. Liu et al demonstrated a PLGA scaffold with mineral gradient generated by a pump mediated injection of calcium phosphate solution[46] (Figure 1.6A). The scaffold was partially submerged in the rising solution so that the amount of mineral depositing on the PLGA fiber is positively related to the time that the scaffold was soaked in the solution. The mineral gradient was characterized by SEM showing thickened collagen fiber, and EDX quantification showed enhancement of the ratio between calcium and carbon (Figure 1.6B-F). Adipose stem cells (ASCs) were seeded onto the scaffold to examine the effect of the mineral gradient on the stem cell behavior. The distribution of cells was homogenous until the 7^{th} day when regions of the scaffold with higher mineral content exhibited lower cell density. Immunocytochemical staining showed that the ALP activity, Runx2 expression and osteocalcin protein (OCN) all have positive relation with culture time and mineral content (Figure 1.7A, B). OCN is a protein hormone specifically found in bone and dentin, which characterizes the mineralization of matrix and late stage differentiation of osteoblasts[47]. These results indicated the mineral gradient has led to different osteogenic behavior of ASCs within the PLGA scaffold. Despite the success in discovering the relationship between mineral content or gradient and stem cell behavior, these synthetic scaffolds did not aim to recapitulate the mineralized collagen matrix within native entheses.

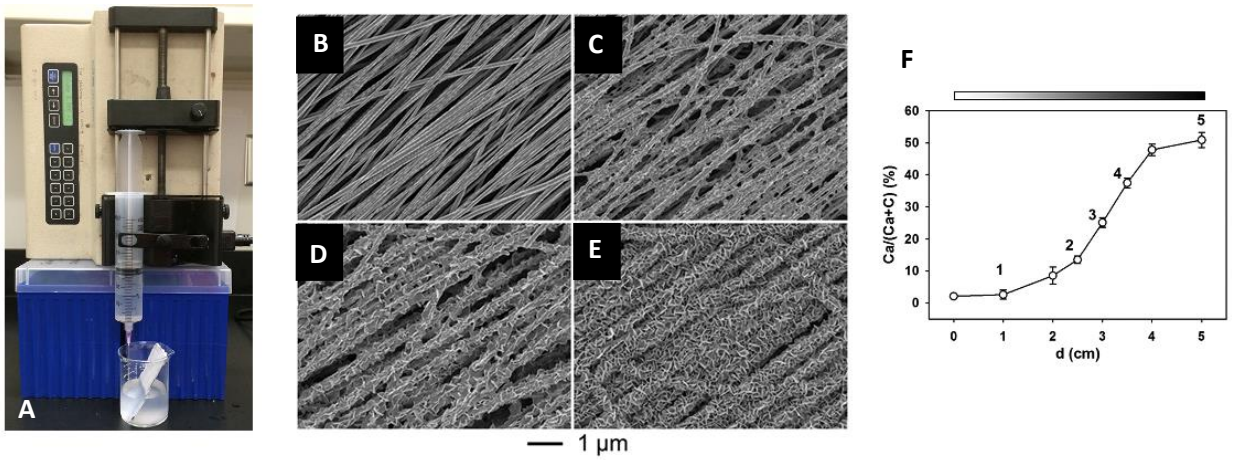

Figure 1.6 A) Setup to generate the mineral gradient in the scaffold. As the calcium phosphate solution is pumped into the beaker, the mineral is deposited on the PLGA nanofiber scaffold. The extent of mineralization is controlled by the time of immersion. B), C), D), E) SEM images of calcium phosphate coated PLGA fiber at 1cm, 2cm, 3cm and 5cm from the less mineralized end. F) EDX quantification of the mineral gradient along the PLGA scaffold (reprinted from Ref. 46 (ACS Applied Material Interfaces), with permission from American Chemical Society).

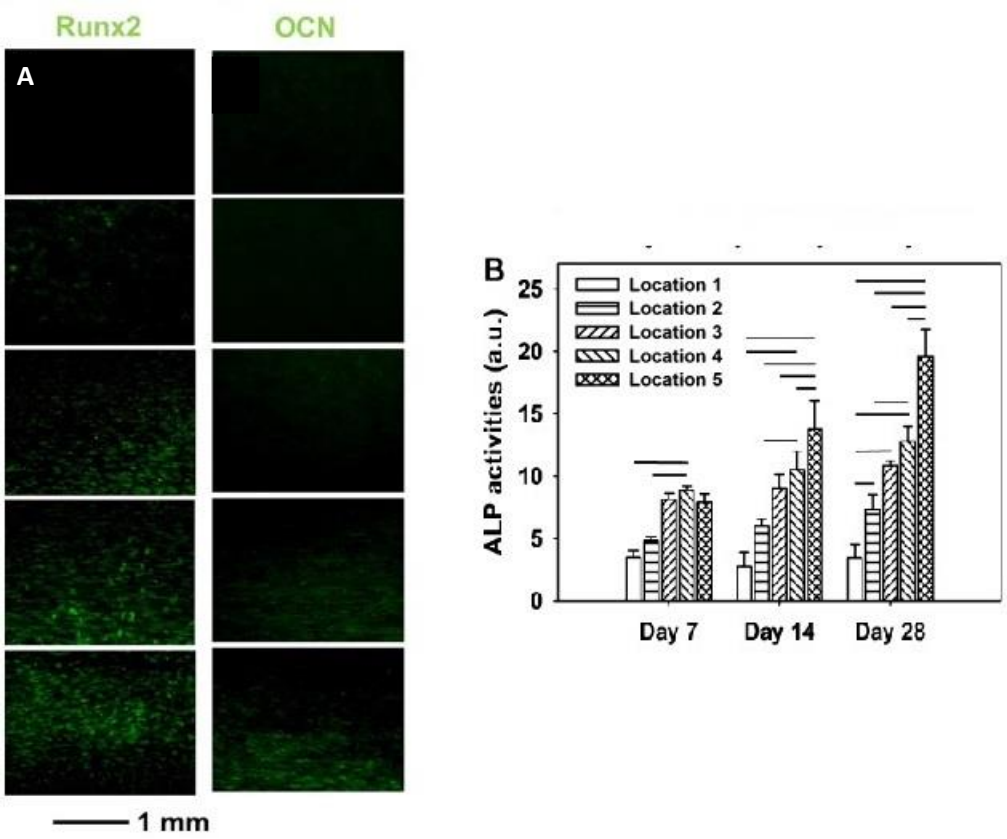

Figure 1.7 A) Runx2 and OCN stainings of adipose stem cells seeded on the scaffold after 28 days. The top is the least mineralized side of the scaffold. The mineralization increases as images moving down. Higher mineralization content results in more significant Runx2 and OCN expression. B) Increasing ALP activity of adipose stem cells seeded on the scaffold measured along mineral gradient over time. Locations 1,2,3,4,5 are as indicated in Figure 1.6F (reprinted from Ref. 46 (ACS Applied Material Interfaces), with permission from American Chemical Society).

Collectively, these studies point to the need for methods to create functionally graded mineralized scaffolds for entheses engineering and better understanding how the mineral gradients affect cellular behavior. Conventional methodologies to fabricate theses scaffolds

followed a 'bottom-up' concept where mineral is deposited onto unmineralized scaffolds. Alternatively, we have developed a 'top-down' method to spatially remove existent mineral from bone matrix[48]. Briefly, we suspended decellularized bone scaffolds partially in an EDTA solution to chelate HAp from the regions submerged in the solution. We demonstrated control over the spatial distribution of mineral in these bone scaffolds by using powder X-ray diffraction (pXRD), histological stainings and micro-computed topography (μCT). In addition, line scans of mineral-to-matrix peak ratio from the mineralized to the demineralized regions of the scaffolds using Raman microscopy revealed compositional mineral gradients at scale around 30μm[48]. These results suggested that the mineral gradients in our scaffolds are comparable to those observed in the native meniscal entheses. We further demonstrated that our scaffolds exhibit low cytotoxicity to MSCs using live/dead stains and support robust MSC attachment using scanning electron microscope (SEM) (Fig. S9). In this thesis, my main objectives are to examine the cellular response to the bone scaffolds *in vitro* and discuss the possibility of applying these scaffolds to the TE meniscus model developed in our group.

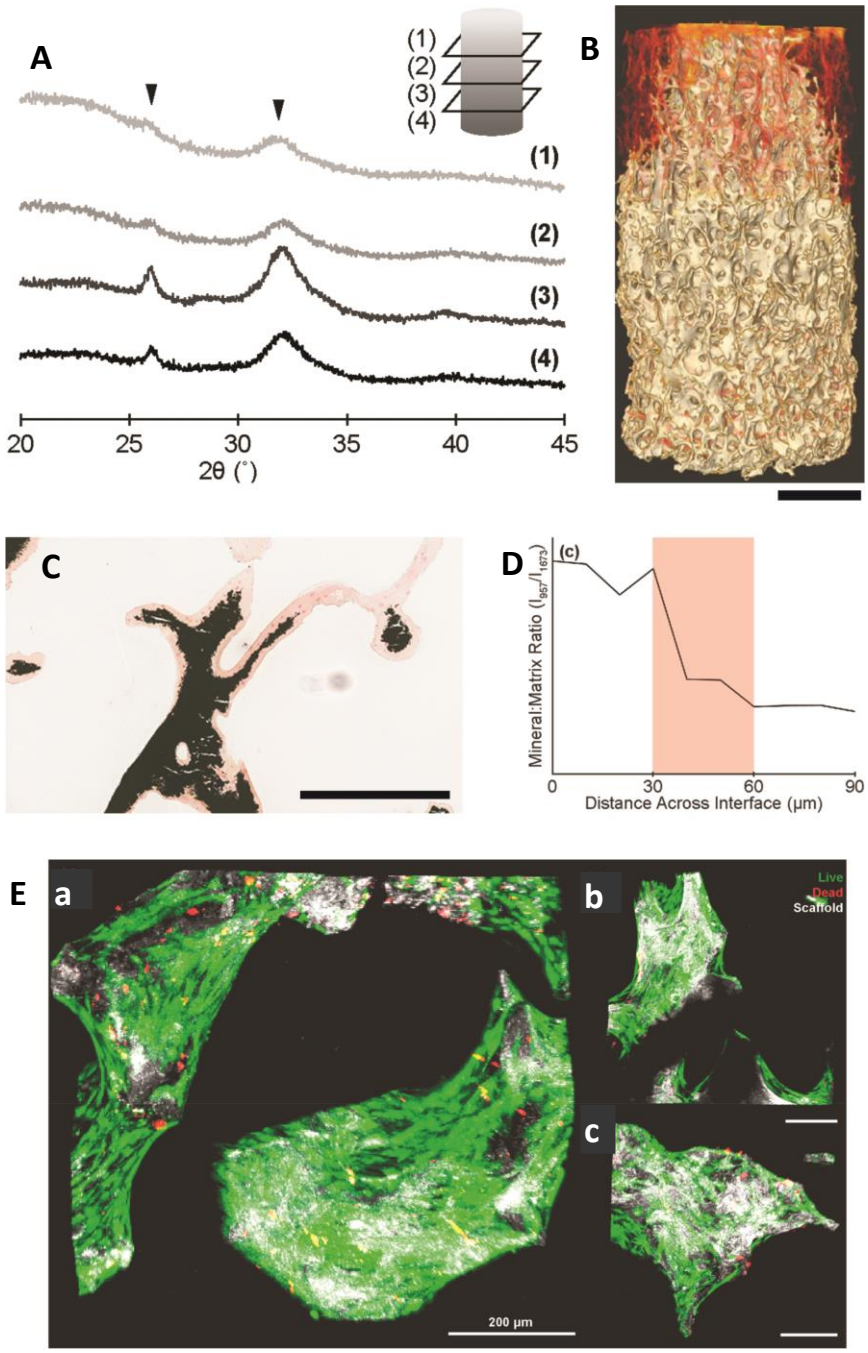

Figure 1.8 A) pXRD shows decreasing hydroxyapatite peaks at 26° and 32° from the bottom mineralized region 4 to the top demineralized region 1 of the scaffolds. B) 3D rendering of the bone scaffold with controlled mineral distribution generated from μCT data. White=Mineral, Red=Collagen. Scale bar=2mm. C) Von Kossa histological staining on a section of the bone

scaffold at the demineralization front. Black=Mineral, Pink=Collagen. Scale bar=500μm. D) Line scan of Mineral-to-Matrix ratio across demineralization front from RAMAN spectroscopic data. Highlighted is the mineral gradient in range of 30 microns. E) Live/dead stains of MSCs seeded on the bone scaffold imaged by confocal microscope at a) mineralized/demineralized interface, b) demineralized region, a) mineralized region. Green=Living cells, Red=Dead Cells, White=Scaffold. Scale bar=200μm (reprinted from Ref. 48 (ACS Biomaterial Science and Engineering), with permission from American Chemical Society).

1.6 References

1. Abraham, A. and Haut Donahue, T. From meniscus to bone: A quantitative evaluation of structure and function of the human meniscal attachments. *Acta Biomater*, 2013. 9(5), pp.6322-6329.

2. Mente, P. and Lewis, J. Elastic modulus of calcified cartilage is an order of magnitude less than that of subchondral bone. *J. Orthop. Res.*, 1994. 12(5), pp.637-647.

3. J.P. Spalazzi, A.L. Boskey, N. Pleshko, and H.H. Lu: Quantitative mapping of matrix content and distribution across the ligament-to-bone insertion. *PLOS ONE*. 8, e74349 (2013).

4. S. Thomopoulos, G.M. Genin, and L.M. Galatz: The development and morphogenesis of the tendon-to-bone insertion. What development can teach us about healing. *J. Musculoskelet. Neuronal Interact*. 10, 35–45 (2010).

5. K. Messner and J. Gao: The menisci of the knee joint. Anatomical and functional characteristics, and a rationale for clinical treatment. *J. Anat*. 193, 161–178 (1998).

6. Lowenstam, H. and Weiner, S. On Biomineralization; *Oxford University Press: Cary*, 1989.

7. Hassenkam, T., Fantner, G., and Hansma, P. High-resolution AFM imaging of intact and fractured trabecular bone. *Bone*, 2004. 35(1), pp. 4-10.

8. Olszta, M., Cheng, X. and Gower, L. Bone structure and formation: A new perspective. *Materials Science and Engineering: Reports*, 2007. 58(3-5), pp.77-116.

9. Wenk, H. and Heidelbach, F. Crystal alignment of carbonated apatite in bone and calcified tendon: results from quantitative texture analysis. *Bone*, 1999. 24(4), pp. 361-369.

10. Benjamin, M.; Moriggl, B.; Brenner, E.; Emery, P.; Mcgonagle, D.; Redman, S. The ?Enthesis Organ? Concept: Why Enthesopathies May Not Present as Focal Insertional Disorders. *Arthritis & Rheumatism*, 2004. 50(10), 3306–3313.

11. Allografts in Sports Medicine: What do we know, need to know, and need to do? Round table discussion: American Orthopedic Society for Sports Medicine; 2006. Park City, UT

12. Holm, I.; Øiestad, B. E.; Risberg, M. A.; Gunderson, R.; Aune, A. K. No Differences in Prevalence of Osteoarthritis or Function After Open Versus Endoscopic Technique for Anterior Cruciate Ligament Reconstruction. *Am. J. Sports Med.*, 2012. 40(11), 2492–2498.

13. Khetia, E. and McKeon, B. Meniscal Allografts: Biomechanics and Techniques. *Sports Med. Arthrosc.*, 2007. 15(3), pp.114-120.

14. Thorlund, J., Hare, K. and Lohmander, L. Large increase in arthroscopic meniscus surgery in the middle-aged and older population in Denmark from 2000 to 2011. *Acta Orthop.*, 2014. 85(3), pp.287-292.

15. Hutchinson, I., Moran, C. and Potter, H. Restoration of the Meniscus. *Am. J. Sports Med.*, 2013. 42(4), pp.987-998.

16. Jeong, H.-J.; Lee, S.-H.; Ko, C.-S. Meniscectomy. *Knee Surg. Relat. Res.*, 2012, 24(3), 129–136.

17. Abrams, G. D.; Frank, R. M.; Gupta, A. K.; Harris, J. D.; Mccormick, F. M.; Cole, B. J. Trends in Meniscus Repair and Meniscectomy in the United States, 2005-2011. *Am. J. Sports Med.*, 2013, 41(10), 2333–2339.

18. Lee, S., Kim, J. and Nam, S. The Tips and Pitfalls of Meniscus Allograft Transplantation. *Knee Surg. Relat. Res.*, 2012. 24(3), pp.137-145.

19. Shelton, W. R.; Dukes, A. D. Meniscus Replacement with Bone Anchors: A Surgical Technique. *Arthroscopy: The Journal of Arthroscopic & Related Surgery*, 1994, 10(3), 324–327.

20. Sekiya J. K., Ellingson C.I. Meniscal allograft transplantation. *J Am Acad Orthop Surg*, 2006. 14(3):164-74.

21. Lee, C., Rodeo, S. and Mao, J. Protein-releasing polymeric scaffolds induce fibrochondrocytic differentiation of endogenous cells for knee meniscus regeneration in sheep. *Sci. Transl. Med.*, 2014. 6(266), pp.266ra171-266ra171.

22. Kang, S., Son, S. and Kim, B. Regeneration of whole meniscus using meniscal cells and polymer scaffolds in a rabbit total meniscectomy model. *J. Biomed. Mater. Res. A*, 2006. 78A(3), pp.638-651

23. Chen, M., Branch, T. and Hutton, W. Is it important to secure the horns during lateral meniscal transplantation? A cadaveric study. *Arthroscopy: The Journal of Arthroscopic & Related Surgery*, 1996. 12(2), pp.174-181.

24. McCorry, M., Mansfield, M. and Bonassar L. A model system for developing a tissue engineered meniscal enthesis. *Acta Biomater*, 2017. 56, pp.110-117.

25. Rho, J., Kuhn-Spearing, L. and Zioupos, P. Mechanical properties and the hierarchical structure of bone. *Med. Eng. Phys.*, 1998. 20(2), pp.92-102.

26. Boys, A., Kunitake, J., Henak, C., Cohen, I., Estroff, L., Bonassar, L. Understanding the stiff-to-compliant transition of the meniscal attachments through correlative raman microscopy and confocal elastography, *ACS Appl. Mater. Interfaces*, 2019. doi: 10.1021/acsami.9b03595.

27. Caplan, A. and Dennis, J. Mesenchymal stem cells as trophic mediators. *J. Cell. Biochem.*, 98(5), 2006. pp.1076-1084.

28. Barry, F., Boynton, R. and Murphy, J. Chondrogenic Differentiation of Mesenchymal Stem Cells from Bone Marrow: Differentiation-Dependent Gene Expression of Matrix Components. *Exp. Cell. Res.*, 2001. 268(2), pp.189-200.

29. Font Tellado, S., Bonani, W. and Van Griensven, M. Fabrication and Characterization of Biphasic Silk Fibroin Scaffolds for Tendon/Ligament-to-Bone Tissue Engineering. *Tissue Eng. Part A*, 2017. 23(15-16), pp.859-872.

30. O'Rahilly, R. Early human development and the chief sources of information on staged human embryos. *Eur. J. Obstet. Gynecol. Reprod. Biol.*, 1979. 9(4), pp.273-280.

31. Thula, T., Rodriguez, D. and Gower, L. In vitro mineralization of dense collagen substrates: A biomimetic approach toward the development of bone-graft materials. *Acta Biomater*, 2011. 7(8), pp. 3158-3169.

32. Papadimitropoulos, A., Scotti, C. and Martin, I. Engineered decellularized matrices to instruct bone regeneration processes. *Bone*, 2015. 70, pp. 66-72.

33. Reddi, A. Morphogenetic messages are in the extracellular matrix: biotechnology from bench to bedside. *Biochem. Soc. Trans.*, 2000. 28(4), pp. 345.

34. Gilbert, T., Sellaro, T. and Badylak, S. Decellularization of tissues and organs. *Biomaterials*, 2006. 27(2006), pp. 3675-3683.

35. Grayson, W., Frohlich, M. and Vunjak-Novakovic, G. Engineering anatomically shaped human bone grafts. *Proc. Natl. Acad. Sci. U. S. A.*, 2009. 107(8), pp. 3299-3304.

36. Grayson, W., Bhumiratana, S. and Vunjak-Novakovic, G. Effects of Initial Seeding Density and Fluid Perfusion Rate on Formation of Tissue-Engineered Bone. *Tissue Eng. Part A*, 2008. 14(11), pp. 1809-1820.

37. Wang, H., Gee, A. and Maher, S. Bone Plug Versus Suture-Only Fixation of Meniscal Grafts. *Am. J. Sports Med.*, 2014. 42(7), pp. 1682-1689.

38. Mauney, J., Blumberg, J. and Kaplan, D. Osteogenic Differentiation of Human Bone Marrow Stromal Cells on Partially Demineralized Bone Scaffolds in-Vitro. *Tissue Eng.*, 2004, 10(1-2), pp. 81-92.

39. Langenbach, F. and Handschel, J. Effects of dexamethasone, ascorbic acid and β-glycerophosphate on the osteogenic differentiation of stem cells in vitro. *Stem Cell Res. Ther.*, 2013. 4(5), pp. 117.

40. Ma, X., Zhang, X. and Wang, Y. Dexamethasone induces osteogenesis via regulation of hedgehog signalling molecules in rat mesenchymal stem cells. *Int. Orthop.*, 2013. 37(7), pp. 1399-1404.

41. Dormer, N. Qiu, Y. and Detamore, M. Osteogenic Differentiation of Human Bone Marrow Stromal Cells in Hydroxyapatite-Loaded Microsphere-Based Scaffolds. *Tissue Eng. Part A*, 2012. 18(7-8), pp. 757-767.

42. Lee, J., Pereira, C. and Miller, T. Optimizing Collagen Scaffolds for Bone Engineering. *J. Craniofac. Surg.*, 2015. 26(6), pp. 1992-1996.

43. Rogina, A., Antunović, M. and Ivanković, H. Human Mesenchymal Stem Cells Differentiation Regulated by Hydroxyapatite Content within Chitosan-Based Scaffolds under Perfusion Conditions. *Polymers*, 2017. 9(12), pp. 387.

44. Chen, J.-P.; Lai, G.-J.; Shalumon, K. Response of Human Mesenchymal Stem Cells to Intrafibrillar Nanohydroxyapatite Content and Extrafibrillar Nanohydroxyapatite in Biomimetic Chitosan/Silk Fibroin/Nanohydroxyapatite Nanofibrous Membrane Scaffolds. *Int. J. Nanomedicine*, 2015, 567.

45. Wang, Y.; Wu, S.; Kuss, M. A.; Streubel, P. N.; Duan, B. Effects of Hydroxyapatite and Hypoxia on Chondrogenesis and Hypertrophy in 3D Bioprinted ADMSC Laden Constructs. *ACS Biomater. Sci. Eng.*, 2017, 3(5), 826–835.

46. Liu, W.; Lipner, J.; Xie, J.; Manning, C. N.; Thomopoulos, S.; Xia, Y. Nanofiber Scaffolds with Gradients in Mineral Content for Spatial Control of Osteogenesis. *ACS Appl. Mater. Interfaces*, 2014, *6*(4), 2842–2849.

47. Huang, W. Signaling and Transcriptional Regulation in Osteoblast Commitment and Differentiation. *Front Biosci*, 2007, 12(8-12), 3068.

48. Boys, A. J.; Zhou, H.; Harrod, J. B.; Mccorry, M. C.; Estroff, L. A.; Bonassar, L. J. Top-Down Fabrication of Spatially Controlled Mineral-Gradient Scaffolds for Interfacial Tissue Engineering. *ACS Biomater. Sci. Eng.*, 2019, 5 (6), 2988–2997.

Chapter 2

Mineral Distribution Spatially Patterns MSC Behavior on Monolithic Bone Scaffolds

2.1 Introduction

The enthesis, the connective tissue attaching soft tissue such as tendon, ligament and meniscus to the bone, is crucial for the biomechanical function of joints[1]. For example, the enthesis provides transosseous fixation while the meniscus mediates the shocks within the knee joint and redistributes the loading into lateral orientations[2]. Operative intervention is usually needed when the enthesis is damaged, and surgeons are required to recreate the transition from soft to hard tissue. The surgical repair of common injuries like rotator cuff and anterior cruciate ligament (ACL) tears are reported to have failure rates ranging from 11% to 95% and postoperative pain within one year among nearly half of the patients[3]. While sutures are widely used to fix soft tissue to bone in most surgical procedures[4-8], it remains challenging to reconstitute healthy entheses, since they consist of transitional tissue with gradients of extracellular matrix (ECM) composition, architecture, cell phenotype and mechanical properties[1]. One key feature within the native enthesis is the hydroxyapatite (HAp) mineral gradient which starts from compliant soft tissue with no mineral moving to the stiff bone with ~ 50 vol% or 65 wt% mineral[9,10]. The presence of mineral stiffens the collagenous ECM and provides multiple orders of magnitude change in modulus over a few hundred microns within the enthesis structure[11-13]. Along the mineral gradient reside distinct phenotypes of cells, which depend on the type of soft tissue. For instance, in the meniscal enthesis, the bone contains osteoblasts, osteocytes and osteoclasts and the meniscus contains fibrochondrocytes, whereas in tendinous enthesis, the soft tissue is populated by fibroblasts[2,14]. Reestablishing the mineral

gradients and the diverse cellular populations are essential to achieve successful repair of entheses.

A number of studies have explored different strategies for enthesis engineering. Previous work has primarily aimed at creating synthetic scaffolds with 'bottom-up' approach in which mineral is deposited in gradients on scaffolds to reproduce the ECM environment of enthesis[15-18]. For example, a mineral gradient was patterned on a polylactic glycolic acid (PLGA) nanofiber scaffold by partially submerging the scaffold in a solution of calcium and phosphate ions to nucleate apatitic mineral[17]. Others focused on producing multiphasic scaffolds by combining different layers of biomaterials[19-21]. Although these scaffolds showed high biocompatibility towards cells, they lack the native transitional structure from bone to soft tissue. Recently, our group has demonstrated a 'top-down' method to create mineral gradient in a trabecular bone scaffold by chelating calcium in a spatially controlled manner[22]. Using decellularized trabecular bone as scaffold has several advantages over synthetic materials. For example, it maintains the native architecture of mineralized collagen, and therefore the mechanical properties of the bone[23]. Demineralized bone can also serve as an appropriate template for the deposition of mineral through biological processes[24].

While the 'top-down' approach is promising, the response of cells to the spatially patterned mineral within scaffolds is not well understood. In the current study, we investigated the effect of mineral distribution within our scaffolds on cellular behavior *in vitro*. Mesenchymal stem cells (MSCs), a therapeutic cell source, were seeded onto the bone scaffold due to their multipotency of differentiating into all cellular phenotypes available in the enthesis[1,14,18,25]. Notably, the osteogenesis and chondrogenesis by MSCs are known to be controlled by HAp[26-30].

Thus, the use of MSCs in these scaffolds containing HAp gradients can potentiate the development of a tissue-engineered enthesis with cellular complexity.

The objective of this work was to control the osteogenesis and chondrogenesis of MSCs in the bone scaffold with spatially controlled distribution of mineral. As the presence of HAp can enhance the osteogenesis by MSCs, we hypothesize that in our model, the osteogenesis would be positively correlated with mineral content in the bone scaffold. In addition, it has been reported that the chondrogenesis by MSCs is conditionally promoted by HAp. Thus, it will be worthy investigating the effect of mineral distribution on the MSC behavior in our scaffolds.

2.2 Methods

2.2.1 Scaffold Fabrication

Cores of trabecular bone were extracted and decellularized as previously described[31]. Briefly, bone plugs were explanted from the distal femurs of 12 1-3 day old neonatal bovines (Gold Medal Packing, Inc., Rome, NY) with a coring bit of 6 mm in diameter. The articular cartilage of the extracted biopsies was removed, and the trabecular parts were sectioned into 10 mm long cylindrical plugs. The cellular debris and bone marrow of the plugs were rinsed off with high velocity stream of deionized water. The bone plugs were soaked sequentially in 0.1 w/v% ethylenediaminetetraacetic acid (EDTA) (TCI, Tokyo, Japan) in phosphate buffered saline (PBS) (Corning, Manassas, VA) for 1 hour at room temperature, hypotonic buffer (10 mM Trizma base (TCI, Tokyo, Japan), 0.1 w/v% EDTA in PBS) at 4°C for 24 hours, and detergent (10 mM Trizma base, 0.5 w/v% sodium dodecyl sulfate (SDS) (Sigma, St. Louis, MO) in PBS) at 4°C for 24 hours. Following washes, biopsies were rinsed thoroughly with PBS. The

decellularized bone plugs were skewered halfway along the long axis of the cylinder on a surgical needle and partially dipped in a 9.5 w/v% EDTA in PBS solution (pH = 7.4) for 4.5 hours to demineralize (Figure 2.1A).

2.2.2 MSC Extraction and Expansion

MSCs were isolated from the trabecular bone marrow in the distal femur of 10 1-3 day old neonatal bovines as previously described[31]. Briefly, the trabecular region of the femur was washed with heparin supplemented media, and the extracted solution was centrifuged at 300 x$\bar{g}$. Pelleted cells were plated on culture flasks and the non-adherent cell population was washed off after 48 hours. Isolated MSCs were plated at a cellular density of 2000 cells/cm^3 and expanded to passage 3 in an expansion media including Dulbecco's modified Eagle's medium without sodium pyruvate (DMEM) (Corning, Manassas, VA), 10% fetal bovine serum (FBS) (Gemini Bio-Products, West Sacramento, CA, 1 ng/mL basic fibroblast growth factor (bFGF) (BD Biosciences, Franklin Lakes, NJ) and 100 IU/mL penicillin (Figure 2.1B). These MSCs showed multipotency through triple lineage test (Fig. S8)

2.2.3 MSC Seeding and Culturing

The demineralized scaffolds were soaked in 70vol% ethanol for 30 minutes, followed by a 1.5 hour wash in PBS and a 2 hour wash in either ***growth media*** composed of Minimum Essential Medium-α (MEM-α) (ThermoFisher, Waltham, MA), 10vol% FBS, 100 IU/mL penicillin or ***osteogenic media*** composed of Minimum Essential Medium-α (MEM-α) (Thermo Fisher, Waltham, MA), 10vol% FBS, 100 IU/mL penicillin, 2 mM L-glutamine (VWR, Brooklyn, NY), 0.1 μM β-glycerolphosphate (MP, Santa Ana, CA), 50 μM ascorbic acid (Sigma, St. Louis, MO), 0.1 μM dexamethasone (Sigma, St. Louis, MO), or ***chondrogenic media***

composed of DMEM (Corning, Manassas, VA), 10vol% FBS (Gemini Bio-Products, West Sacramento, CA), 100 IU/mL penicillin, 1mM non-essential amino acids (Invitrogen, Thermo Fisher, Waltham, MA), 0.4 mM L-proline (Sigma, St. Louis, MO), 50μm/mL ascorbic acid. The bone scaffolds were seeded with MSCs as previously described. Briefly, the bone scaffolds were skewered and suspended in a spinner flask. The flask was supplied with 150 mL of either growth media, osteogenic media, or chondrogenic media at an initial cellular density of 500,000 cells/scaffold and incubated for 48 hours at 37°C, 5% CO_2. After seeding, the scaffolds were transferred into either osteogenic media, growth or chondrogenic media with 10ng/mL transforming growth factor β1 (TGF-β1) (Thermo Fisher Scientific, Waltham, MA) and cultured statically for 4, 7 and 14 days. The cultured scaffolds were fixed in formalin for 24 hours and stored in 70% ethanol (Fig. 2.1C, D).

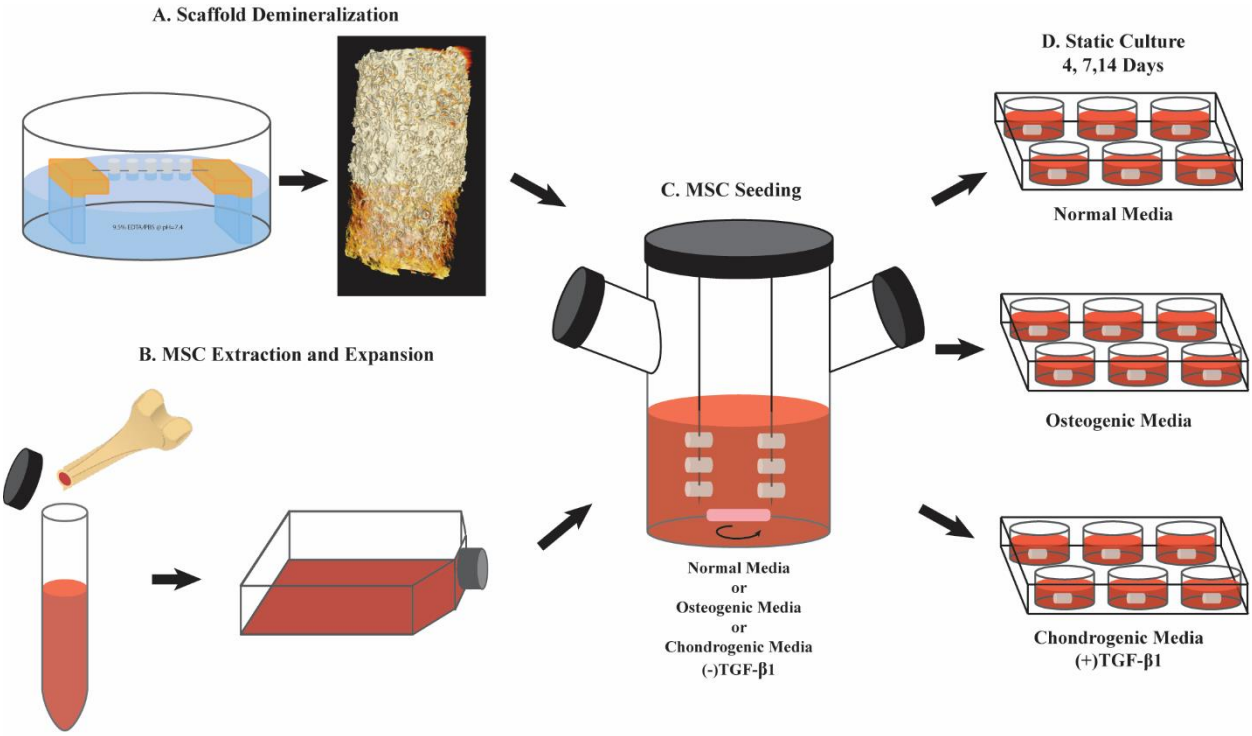

E. IHC Characterization

Osteogenic Markers	Chondrogenic Markers	Hypertrophic Markers	Fiber Formation
Collagen I	GAGs	Collagen X	Collagen I
OCN	Collagen II		Polarized Picrosirius Red
ALP			

Figure 2.1. A) The mineral gradient is produced by demineralizing part of the bone scaffold in EDTA solution. Nano-computed topography showed the demineralized collagen matrix in orange and mineralized regions in white. (reprinted from Ref. 48 (ACS Biomaterial Science and Engineering), with permission from American Chemical Society). B) MSCs are extracted from trabecular bone of neonatal bovine, cultured and expanded to Passage 3. C) Scaffolds were seeded with MSCs in a spinner flask supplied with growth media, osteogenic media and chondrogenic media without TGF-β1 for 48 hrs. D) Seeded scaffolds were statically cultured in well plates supplied with growth media, osteogenic media and chondrogenic media

with TGF-β1 for 4, 7 and 14 days. E) Biomarkers examined by immunohistochemical staining and histological staining.

2.2.4 Histology

Seeded bone scaffolds were fixed, decalcified, dehydrated, embedded in paraffin, sectioned, and stained. Hematoxylin and Eosin (H&E) and Picrosirius Red with Hematoxylin were used to show collagenous matrix in trabecular bone. Alcian Blue and nuclear fast red were used to stain glycosaminoglycans (GAGs) that are deposited by MSCs in scaffolds cultured with chondrogenic media. Sections were imaged using an Aperio Scanscope slide scanner (Aperio Technologies, Inc., Vista, CA) under brightfield illumination. Picrosirius Red stained slides were also imaged under cross-polarizers with a Nikon Eclipse TE2000-S microscope (Nikon Instruments, Melville, NY) and a SPOT RT camera (Diagnostic Instruments, Steriling Heights, MI) to view the alignment of collagen fibrils deposited by MSCs. Images of Alcian blue and nuclear fast red stains was quantified by ImageJ. Briefly, an optimized color deconvolution threshold was created to split the original images into 3 8-bit images containing only Alcian blue stain, nuclear fast red stain and a residue image respectively[32] (Appendix 3.2). The intensity of the Alcian blue stain was evaluated by the IHC profiler plugin. Resultant scores were generated to describe the amount of GAGs stained by Alcian blue in the region of interest (ROI)[33] (Fig. S4).

2.2.5 Immunohistochemical (IHC) Staining

IHC staining was performed on fixed samples embedded in paraffin to study the cellular behavior and the matrix deposited by the MSCs. Following deparaffinization, the sections were treated with citric buffer at 60°C water and 3vol% H_2O_2 at room temperature to retrieve the

antigens. The slides were incubated in blocking serum at room temperature for 1 hour to inhibit unspecific binding of antibodies. The slides were rinsed 5 times in Tris buffer and incubated overnight with rabbit anti-COL1 (1:500) (Abcam, ab34710), , rabbit anti-COL2 (1:500) (Abcam, ab34712), rabbit anti-COLX (1:1000) (Abcam, ab58632), mouse anti-alkaline phosphatase (1:250) (Abcam, ab116592) and mouse anti-osteocalcin (1:250) (ab13420) primary antibodies at 4°C. After rinsing off the primary antibody solution, the slides were incubated in secondary antibody (either rabbit or mouse IgG) solution for 1 hour and avidin-biotinylated horseradish peroxidase for 30 minutes. Following the incubation, the slides were treated with 3,3'-diaminobenzidine (DAB) peroxidase substrate (Vector Laboratories, Burlingame, CA) until brown precipitate was observed in the droplet. The reaction was ceased by rinsing specimens with deionized water. Hematoxylin was used as counterstain to visualize the original bone matrix and cell nuclei. Images of stained by the DAB was quantified by ImageJ using plugins and macros. Briefly, an optimized color deconvolution threshold was created to split the original images into 3 8-bit images containing only DAB stain, hematoxylin stain and a residue image respectively[32] (Appendix 3.1). The intensity of the brown DAB stain was evaluated by the IHC profiler plugin. Resultant scores were generated to describe the amount of specific antigen presenting in the images[33] (Fig. S8).

2.2.6 Statistical Analysis

All quantitative data were expressed as mean ± standard deviation within groups. Pairwise comparisons between treatment groups were conducted using ANOVA test and Tukey's post-hoc test. Significance of scores between different static culture time points is denoted by '#'. Significance of scores between mineralized and demineralized regions is denoted

by '*'. P values less than 0.05 are indicated by single symbol and P values less than 0.01 are indicated by double symbols.

2.3 Results

We investigated the effect of mineral distribution on the behavior of MSCs in our scaffolds containing spatial mineral distribution. MSC-seeded scaffolds were cultured in either growth media, osteogenic media or chondrogenic media. Osteogenic, hypertrophic and chondrogenic biomarkers within MSCs and the matrix they deposited were examined by histological and IHC staining. We also quantified the staining using ImageJ plugins. We compared the behavior of MSCs attaching to the mineralized and demineralized regions of the scaffolds based on the observation on the stained tissue and statistical analysis of staining. In addition, since samples went through decalcification prior to being embedded in paraffin, the mineralized part of the sample could not be distinguished from the demineralized part through brightfield microscopic imaging. As previously described, part that was mineralized showed greener colors when stained with picrosirius red and observed through crossed polarizers. Therefore, polarized light images of slides stained by picrosirius red were used to determine the mineralization condition within specific regions of the scaffolds.

Osteogenic behavior of MSCs cultured in growth media was characterized to understand the effect of mineral distribution on the differentiation of MSCs at 4, 7, 14 days after seeding (Fig. 2.2). Alkaline phosphatase (ALP) was used as an early marker of osteogenesis. By 4 days of static culture in growth media, more intense ALP stain was observed within the matrix deposited by MSCs in the mineralized region of the scaffold than that in the demineralized

region of the scaffold. The ALP expression by MSCs in both sides of the scaffold maintained until day 14 when a decrease of ALP stain was observed (Fig. 2.2 Column B).

To further characterize the osteogenesis within the scaffold, osteocalcin (OCN) IHC stain was used as a late marker of osteoblast differentiation. Stronger OCN staining was observed within MSCs residing the mineralized side of the scaffold as early as day 4 of static culture and the staining intensified at day 14. In contrast, OCN expression was muted on the demineralized side of the scaffold until day 14 when a small amount of OCN staining was observed within the cellular matrix deposited by MSC (Fig. 2.2 Column C). Our observations matched with the OCN scores analyzed by ImageJ (Fig. 2.5A, B).

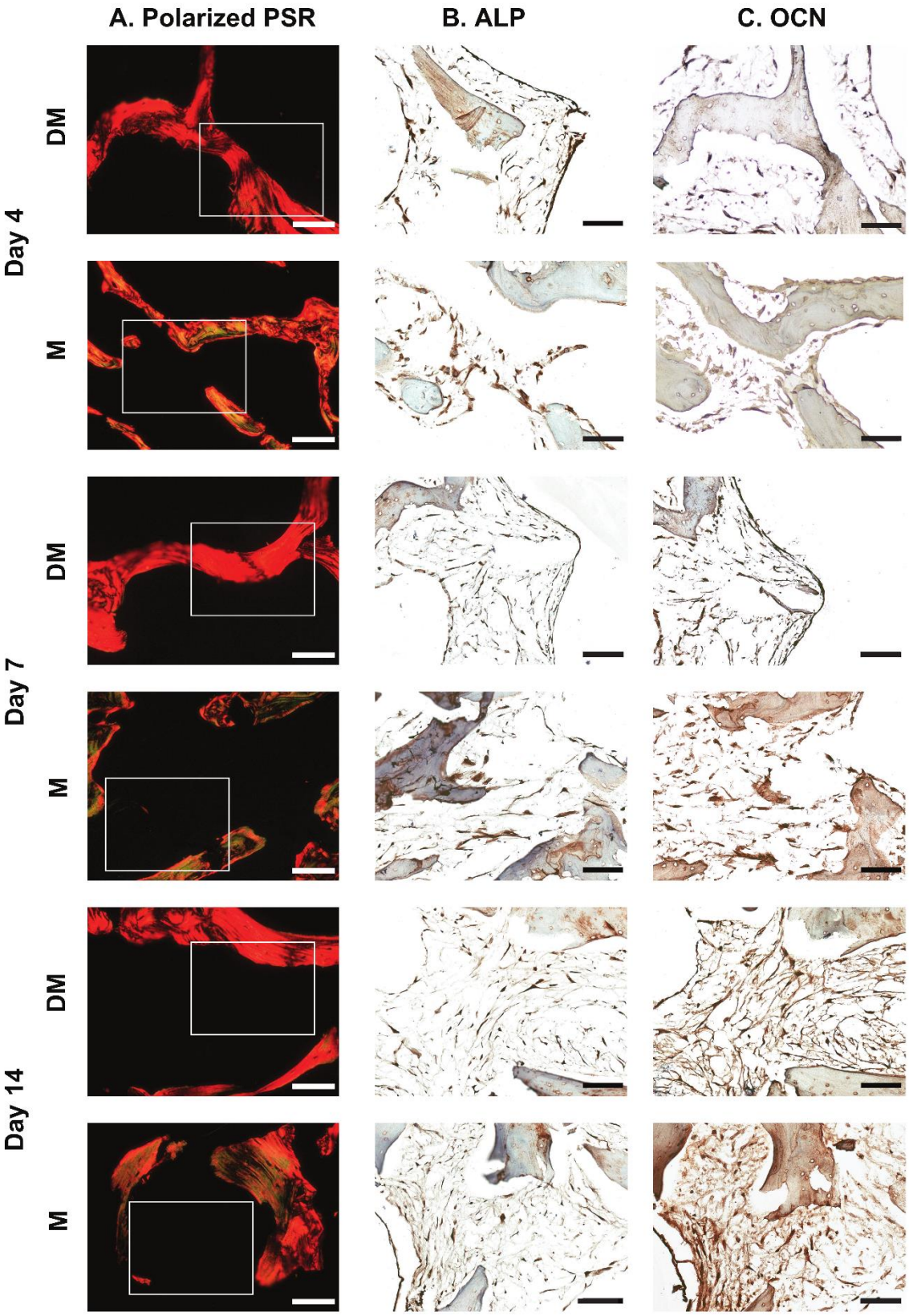
A. Polarized PSR
B. ALP
C. OCN
Day 4
Day 7
Day 14
DM
M
DM
M
DM
M

Figure 2.2 Light microscope images of Picrosirius red (Fig. S1 Column A) and IHC stained seeded scaffolds cultured in growth media. Each pair of M (mineralized) and DM (demineralized) images are from one scaffold, different regions. Column A) Seeded scaffold stained by Picrosirius red, observed through crossed polarizers. Mineralized regions showed green color. Demineralized regions showed red color. Scale bars are 200 μm. Column B) Seeded scaffold stained for ALP. Column C) Seeded scaffold stained for OCN. Scale bars are 100 μm. Images in the same row from Columns B) and C) were taken from serial sections in the regions highlighted in Column A).

To analyze the effects of different media components on MSC behavior, MSCs were cultured in osteogenic media. Both ALP and OCN were observed at high intensity in mineralized and demineralized regions of the scaffolds at days 4 and 7. Notably, aggregation of MSCs was observed expressing strong ALP and OCN in the mineralized region of the scaffold (Fig. 2.2 Column C, highlighted in red circle). These cellular structures resemble the direct formation of new trabecular bone[34]. Following that, the intensity of both stains reduced significantly by day 14 (Fig. 2.2 Columns B, C). The IHC scores suggest that the intensity of ALP and OCN stains in the mineralized regions continuously decreased over time while the OCN stains in the demineralized regions peaked at day 7 (Fig. 2.5C, D). This result indicates a delayed osteogenic behavior of MSCs in the demineralized regions.

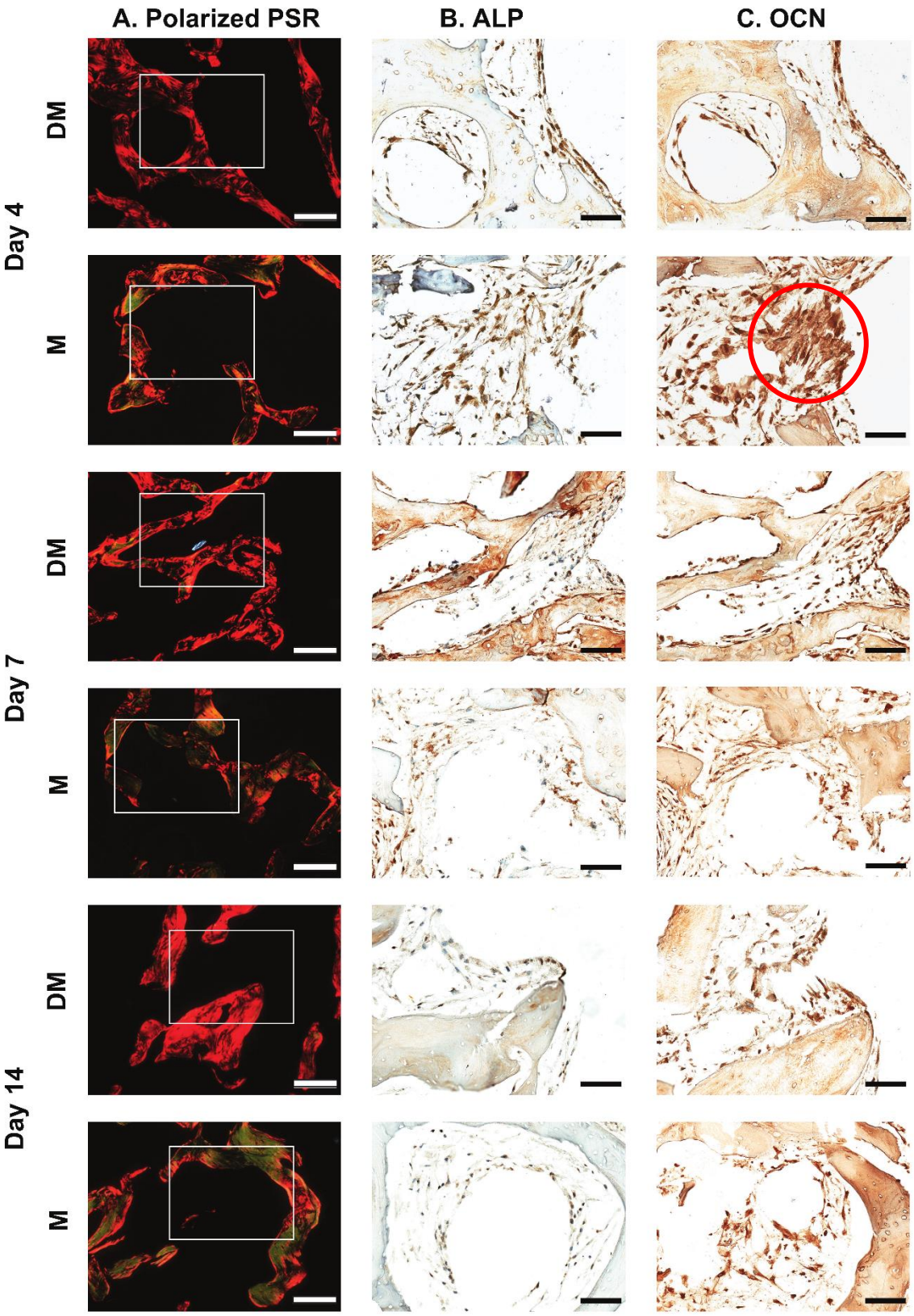
A. Polarized PSR
B. ALP
C. OCN
Day 4
DM
M
Day 7
DM
M
Day 14
DM
M

Figure 2.3 Light microscope images of Picrosirius red (Fig. S1 Column B) and DAB stained seeded scaffolds cultured in growth media. Each pair of M (mineralized) and DM (demineralized) images are from one scaffold, different regions. Column A) Seeded scaffold stained by Picrosirius red, observed through crossed polarizers. Mineralized regions showed green color. Demineralized regions showed red color. Scale bars are 200 μm. Column B) Seeded scaffold stained for ALP. Column C) Seeded scaffold stained for OCN. Scale bars are 100 μm. Images in the same row from Columns B) and C) were were taken from serial sections in the regions highlighted in Column A).

Chondrogenic behavior of MSCs cultured in a chondrogenic biochemical environment containing TGF-β1 was assessed at days 4, 7 and 14 of culture. Histological stain of Alcian blue was used to examine the production of glycosaminoglycans by MSCs. IHC stains of collagen type II and X were used to examine the cartilage-related matrix deposition and hypertrophic differentiation of MSCs. Throughout the 14 days of culture, we did not observe significant Alcian blue staining within the scaffold (Fig. S3-5) while increasing collagen type II and X stains were both detected within the cellular matrix deposited within both regions of scaffolds over time (Fig. 2.3 Columns B, C). Since the deposition of collagen type X was related to the hypertrophic differentiation of MSCs, we suspect the MSCs undergo osteogenic differentiation even when subjected to a chondrogenic biochemical environment. Therefore, IHC stains of OCN and ALP were performed on seeded scaffolds cultured with chondrogenic media. Indeed, we observed more intense OCN stains but less strong ALP stain in the mineralized regions of the scaffold by day 4 of the static culture (Fig. 2.3 Columns D, E). Interestingly, ALP and OCN stains at both regions of the scaffolds kept decreasing over time. MSCs within the demineralized

region of the scaffold was eventually muted in OCN expression by day 14 while showing slightly positive ALP expression. In mineralized regions, MSCs maintained positive OCN stain. These observations matched with the scores analyzed by ImageJ (Fig. 2.5E, F).

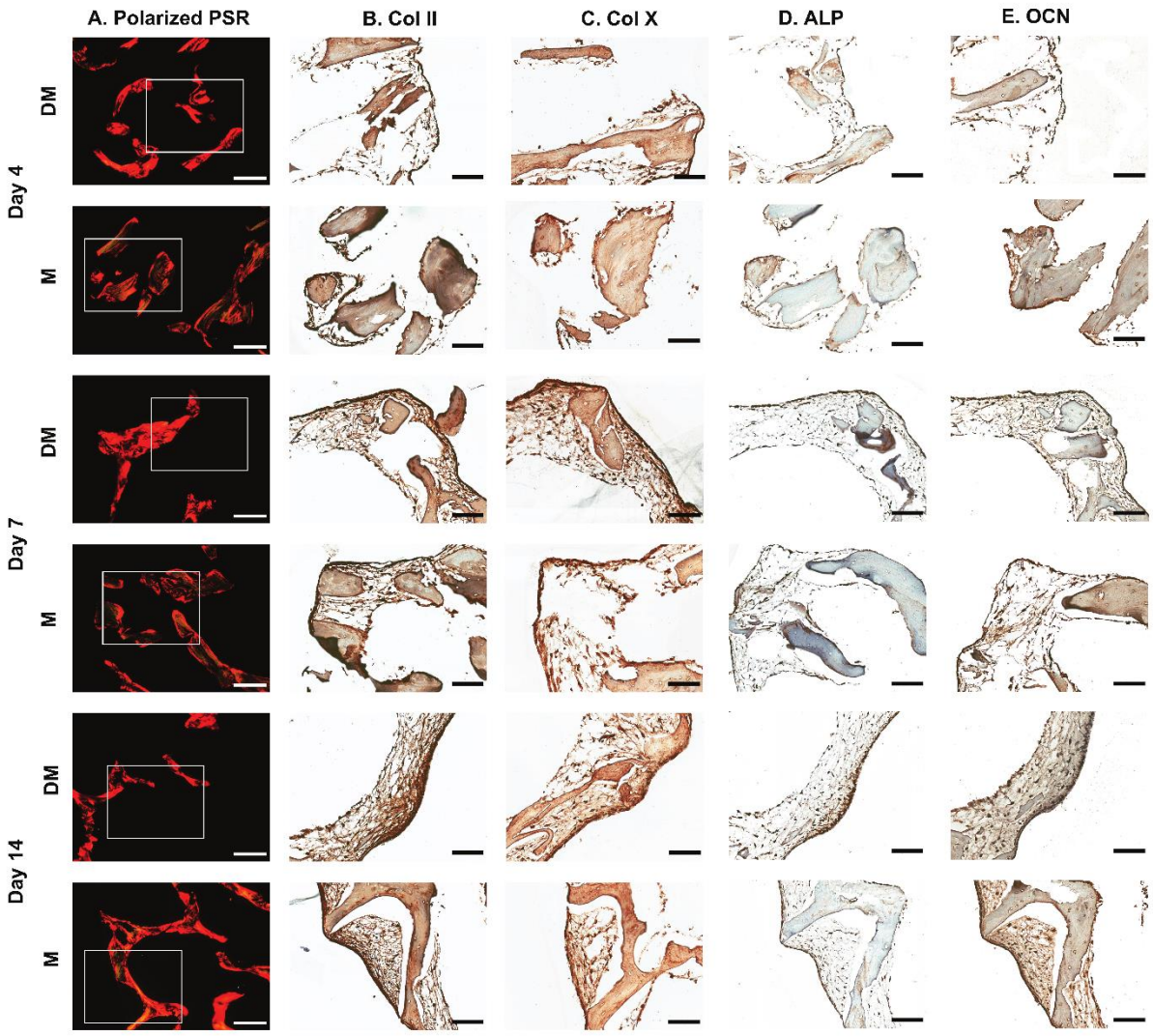

Figure 2.4 Light microscope images of Picrosirius red (Fig. S1 Column C) and DAB stained seeded scaffolds cultured in chondrogenic media. Each pair of M (mineralized) and DM (demineralized) images are from one scaffold, different regions. Column A) Seeded scaffold

stained by Picrosirius red, observed through cross polarizer. Mineralized regions showed green color. Demineralized regions showed red color. Scale bars are 200 μm. Column B) Seeded scaffold stained for Col II. Column C) Seeded scaffold stained for Col X. D) Seeded scaffold stained for ALP. E) Seeded scaffold stained by for OCN. Scale bars are 100 μm. Images in the same row from Column B), C), D) and E) were taken from serial sections in the regions highlighted in Column A).

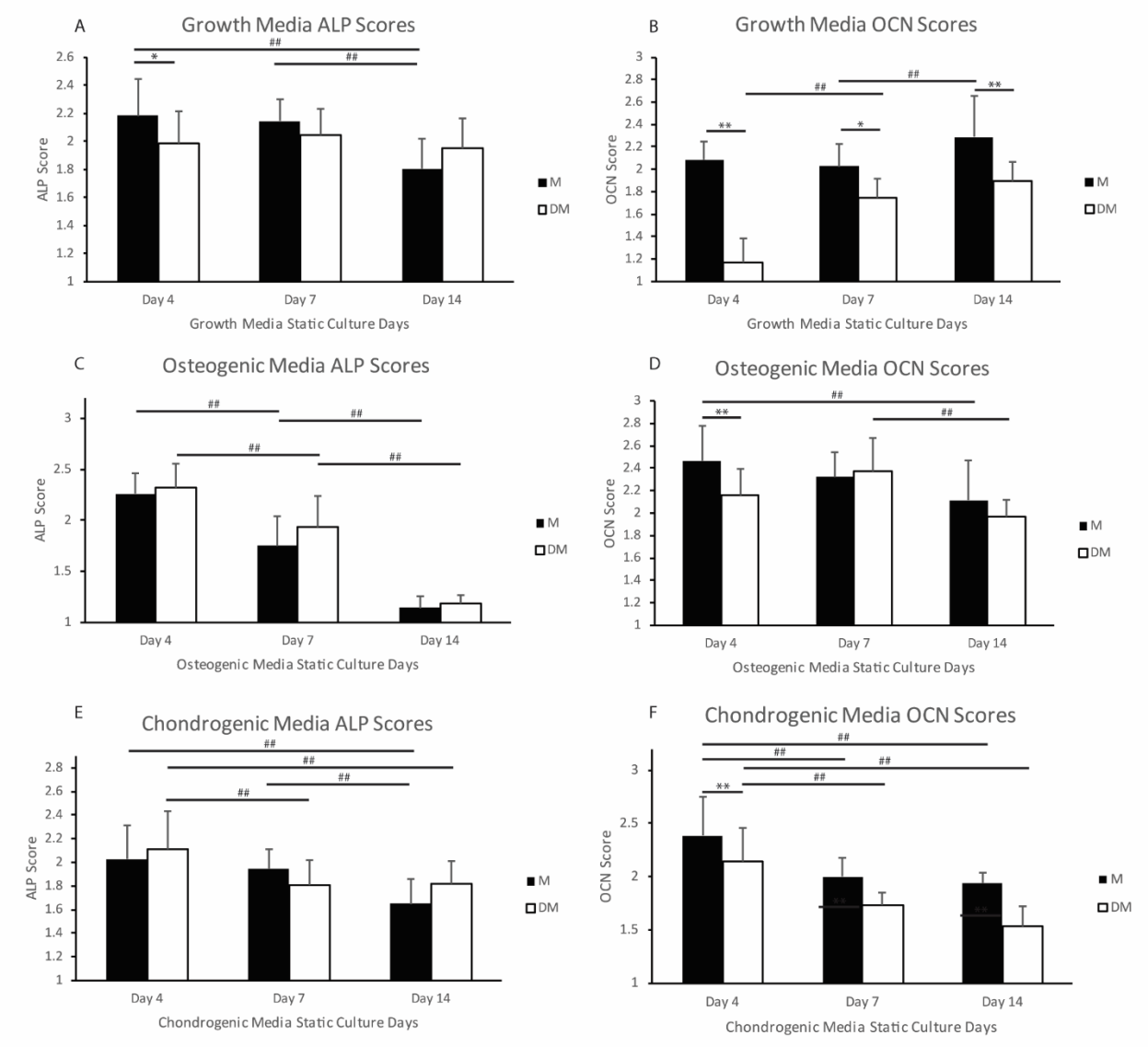

Figure 2.5 ALP and OCN scores of seeded scaffolds cultured in growth, osteogenic and chondrogenic media quantified by ImageJ. Significance of scores between different static culture time points is denoted by '#'. Significance of scores between mineralized and demineralized regions is denoted by ''. P values less than 0.05 are indicated by single symbol and P values less than 0.01 are indicated by double symbols. (n=20)*

In addition to characterizing the differentiation behaviors of MSCs, the formation of collagen fiber was observed on tissue stained by picrosirius red imaged through crossed polarizers. The most prominent fiber formation was observed in MSCs cultured in osteogenic media. By day 4, no significant color from fiber stained by picrosirius red was able to be observed at both sides of the scaffold (Fig. 2.6 Column A). At days 7 and 14, thick layers of collagen fibers formed at the demineralized side of the scaffold which displayed red color while fewer new collagen fibers were observed from the mineralized side of the scaffold, which showed more green color (Fig. 2.6 Columns B, C).

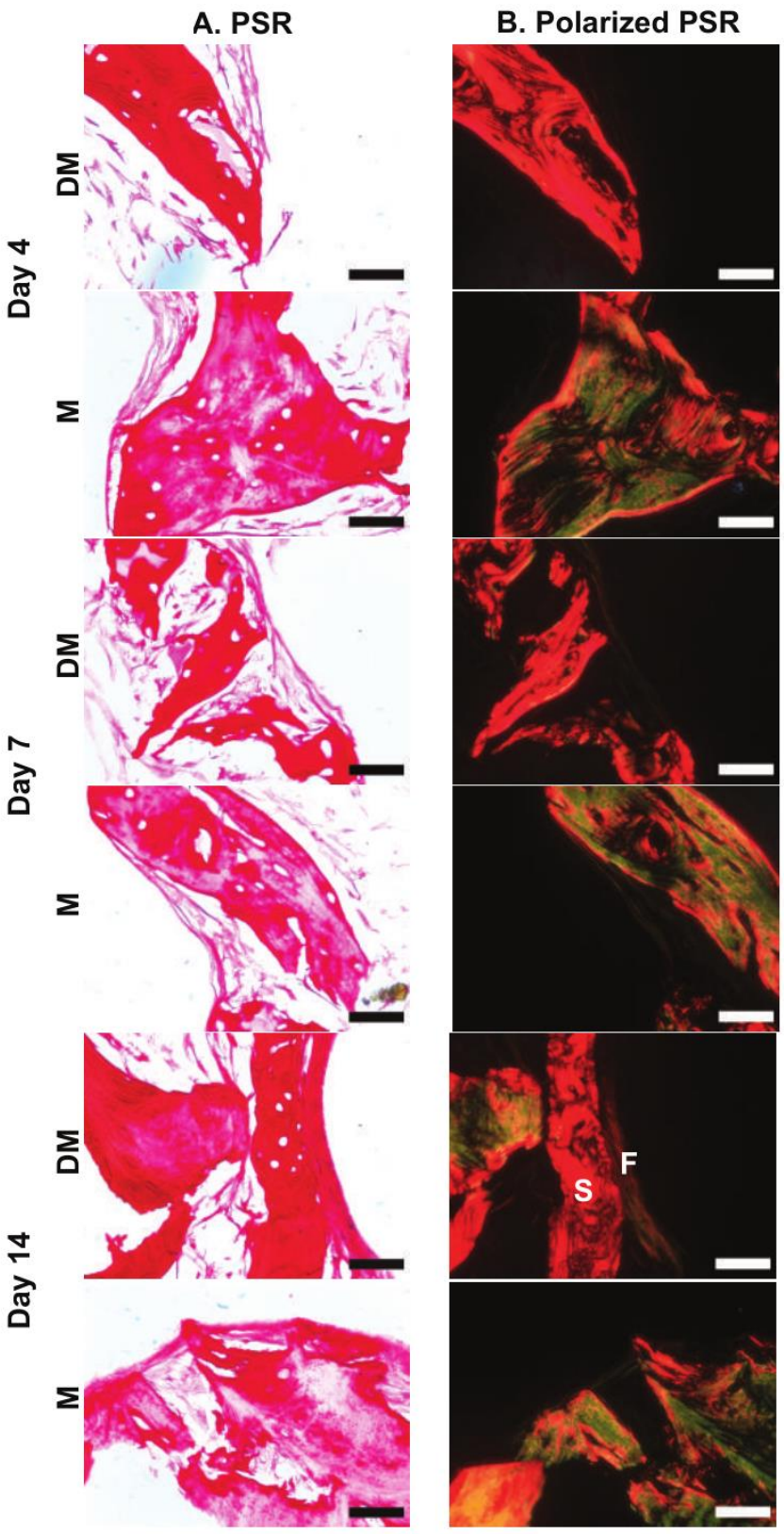
A. PSR
B. Polarized PSR
Day 4
DM
M
Day 7
DM
M
Day 14
DM
M
F
S

Figure 2.6 Picrosirius red stained seeded scaffolds cultured in osteogenic media at Column A) Day 4, Column B) Day 7, Column C) Day 14. For each paired row of M (mineralized) or DM (demineralized), the top images show the Picrosirius red stain under brightfield. The bottom images show the Picrosirius red stain observed through cross polarizer. Mineralized regions showed green color. Demineralized regions showed red color. F=fiber deposited by MSCs. S=Scaffold. Scale bars are 50 μm. Each pair of M and DM images are from one scaffold, different regions.

2.4 Discussion

We have demonstrated spatially controlled osteogenesis by MSCs cultured on the scaffolds with arranged mineral distribution. Two biomarkers of osteogenic differentiation expressed by the MSCs, ALP and OCN were assessed through IHC stainings. ALP signifies the maturation of osteoprogenitors and discerns them from the immature stage[35]. OCN marks the mineralization of ECM and the differentiated stage of osteoblast[35]. ALP and OCN can be used to gauge the differentiation of osteoblastic lineage ranging from mature osteoprogenitor to differentiated osteoblasts[35]. Other osteogenic biomarkers were not used since they either lack clear indication of the specific stage in osteogenic differentiation (e.g. Runx2) or defined detectable ranges (e.g. osteopontin)[35]. When the MSC-seeded scaffolds were cultured in an unbiased biochemical environment (i.e. growth media), MSCs expressed increasing OCN in the regions with high mineral content over time. In contrast, MSCs in the demineralized regions did not express osteocalcin until day 14 of the culture. The addition of osteogenic biochemical cues (e.g. dexamethasone, β-glycerophosphate and ascorbic acid) increases the overall osteogenic behavior of MSCs in the entire scaffolds. As demonstrated by ALP and OCN IHC staining score,

we still noticed that osteogenesic behavior of MSCs was delayed in the demineralized regions of the scaffold by day 4. The difference in terms of osteogenesis between MSCs in the mineralized and demineralized regions of the scaffold, however, diminished by day 7. Therefore, we showed spatial control over MSC osteogenesis patterned by the mineral distribution in our bone scaffold.

Osteogenesis of MSCs promoted by the presence of mineral has been consistently reported by others, Researchers have shown that osteogenesis by MSCs in terms of calcium deposition and ALP activities was enhanced by the presence of mineral in poly(l-lactic acid)(PLLA)/alginate scaffolds[36]. Others have demonstrated the enhanced OCN expression and cuboidal phenotype of adipose stem cells (ACSs) cultured on mineralized PLLA/Poly-benzyl-l-glutamate/Collagen scaffold[27]. Our results, in terms of spatially controlled osteogenesis by stem cells in a monolithic scaffold cultured in both growth and osteogenic media, also aligned with the findings by other researchers. For example, increasing osteogenesis by ASCs was found along a mineral gradient deposited in a PLGA scaffold[17]. Interestingly, compared to stem cells cultured within these synthetic scaffolds, MSCs cultured on our bone scaffold exhibited more rapid osteogenesis in growth media. Other studies have report stem cells in the most mineralized regions of their scaffolds showing osteogenic markers including OCN and ALPs by day 7 of the cultures[16,17,51]. We were able to detect OCN expression within cells and cellular matrix by day 4 of the culture in the mineralized regions of the scaffolds. In addition, the MSCs in the demineralized regions of the scaffold showed OCN markers at day 14 of the static culture in contrast to the negative OCN expression of ASCs in the unmineralized region of the PLGA scaffold as previously observed[17]. Indeed, decellularized bone matrix is known to induce osteogenesis by stem cells naturally even being demineralized since it may contain ECM-associated growth factors. The preservation of these growth factors, however, depends on how

the biopsy is process into the scaffold[24]. We have previously shown our decellularization and demineralization process maintained the underlying protein matrix of the trabecular bone[22]. Therefore, it is possible that the ECM-associated growth factors, mostly composed of proteins were preserved in our scaffolds as well.

We also examined how the spatially controlled mineral distribution in our scaffold affected the MSC behavior in a chondrogenic environment. We firstly examined cellular phenotype and two chondrogenic biomarkers, collagen type II and GAGs. Although MSCs exhibited increasing collagen type II production over time, they deposited little GAG in both the mineralized and demineralized regions of the scaffold. Meanwhile, upregulation of collagen type X, ALP and OCN within MSCs was found by IHC stainings. These results indicate that the MSCs seeded in the scaffold undergo hypertrophic and osteogenic differentiation in the chondrogenic biochemical environment. Additionally, the decreasing osteogenic biomarkers at days 7 and 14 in both regions of the scaffolds can be explained by the addition of TGF-β1 in static culture media which suppresses osteogenesis by MSCs[39]. Despite being suppressed in osteogenic biomarkers, MSCs in the mineralized regions of the scaffold still showed more intense OCN staining than those in the demineralized regions by the end of the culture. This observation implies that the osteoinductive properties of mineralized regions in our scaffolds was maintained even in a chondrogenic biochemical environment.

Chondrogenesis of MSCs has been reportedly influenced by the presence of mineral along with other physical or biochemical cues. Researchers have showed that the chondrogenesis by MSCs enhanced when cultured in hyaluronic acid (HA)/gelatin hydrogel containing 10wt% HAp [28]. Lower concentration of HAp in the hydrogel resulted in downregulation of collagen type II and GAGs production while higher concentration of HAp led to hypertrophic to osteogenic

differentiation. Our observation of cellular behavior in mineralized regions of the scaffolds agreed with their findings as hypertrophic and osteogenic biomarkers were detected. We did not observe evidence, however, of robust chondrogenesis even in the demineralized regions of the scaffold. Notably, chondrogenic differentiation of MSCs depends on the scaffold as well. Scaffolds made from hydrogel showed superior chondroinductive properties compared to porous scaffold such as demineralized bone matrix[40]. We also expect that the injection of hydrogel material to the pores of the scaffold will enhance the chondrogenesis by MSCs since hydrostatic pressure can improve the chondrogenic characteristics of demineralized bone matrix[41].

Collagen fibers deposited by the MSCs at both sides of the scaffold exhibited different colors when stained by picrosirius red and observed through crossed polarizers. The red colors of the collagen fibers at the demineralized side indicate collagen bundles of increasing diameter or alignment[37,38]. Since we aim to integrate the demineralized region of the scaffold with injectable material such as cellular or acellular collagen gel[18], the formation of thicker or more aligned collagen fibers by MSCs in the demineralized regions of the scaffolds may help to improve the integration at the bone-gel interface.

Demineralized bone matrix derived from animal models has been used to study applications in stem cell therapy and bone tissue engineering *in vitro* and *in vivo*[42-44]. In this work, we selected a bovine model of high relevance to research in soft-hard tissue interface[45,46]. Notably, neonatal bovine was used as a source for the scaffolds since its femoral bone mineral density is more comparable to healthy human bone[47]. Therefore, the cellular responses toward the mineral content in our scaffold may be similar to those in the native human trabeculae. In addition, MSCs derived from bovine bone marrow were used to study cellular interaction with the bone scaffold in this study. Although significant difference in cell surface markers has been

observed between bovine MSCs and human MSCs[48], similar cellular behaviors in terms of osteogenic and chondrogenic differentiation have been reported when they are seeded on bone matrix derived from the bovine model[49,50]. Future experiments involving the application of human cells may reveal the feasibility of using these scaffolds to repair entheses in the human model.

Several limitations of this study are to be addressed before we incorporate the scaffold with soft material to fabricate a complete tissue engineered enthesis. In this study, IHC, a qualitative method was used to characterize MSC behavior. To further confirm their behavior in the scaffolds with mineral gradient quantitatively, more powerful tool, for example, biomarker assays and Western blots will be used for quantification of higher accuracy. Furthermore, the mineral content and the stiffness of the scaffold are two dependent variables. Both variables are known to play roles in inducing osteogenesis of MSCs. Using our current fabrication technique, we are not able to isolate one variable from the other. Therefore, the presence of HAp in the scaffold may not be the sole factor that controlled the osteogenesis in this work.

2.5 Conclusion

This work investigated the osteogenic behavior of MSCs cultured on scaffolds with apatitic mineral gradients. We found that the mineral distribution controlled the osteogenic behavior of MSC spatially with or without osteogenic biochemical cues. MSCs in the regions of high mineral content showed upregulated osteogenesis, whereas MSCs in regions of low mineral content showed muted osteogenesis in absence of those cues or delayed osteogenesis when supplied with osteogenic biochemical cues. Additionally, MSCs at the demineralized side of the scaffold produced thicker and more aligned fibers. We further examined the capability of the

scaffold to induce chondrogenesis. Although the MSCs were subjected to a chondrogenic biochemical environment, they still showed osteogenesis controlled by the spatially arranged mineral content. This work demonstrated that our scaffolds with mineral gradients can be used to introduce cellular complexity by tuning osteogenic behavior of MSCs. It shows promising results to improve the ECM biomimicry, soft-hard tissue integration and cellular complexity of the tissue engineered meniscal enthesis developed in our lab.

2.6 References

1. Boys, A., Bonassar, L. and Estroff, L. Next generation tissue engineering of orthopedic soft tissue-to-bone interfaces. *MRS Commun.*, 2017. 7(3), pp.289-308.

2. K. Messner and J. Gao. The menisci of the knee joint. Anatomical and functional characteristics, and a rationale for clinical treatment. *J. Anat*, 1998. 193, 161–178.

3. Apostolakos, J., Durant, T. J., Dwyer, C. R., Russell, R. P., Weinreb, J. H., Alaee, F., Beitzel, K., McCarthy, M. B., Cote, M. P., Mazzocca, A. D. (2014). The enthesis: a review of the tendon-to-bone insertion. *Muscles Ligaments Tendons J.*, *4*(3), 333-42.

4. Lee, S. R.; Kim, J. G.; Nam, S. W. The Tips and Pitfalls of Meniscus Allograft Transplantation. *Knee Surg. Relat. Res.*, 2012, *24*(3), 137–145.

5. Shelton, W. R.; Dukes, A. D. Meniscus Replacement with Bone Anchors: A Surgical Technique. *Arthroscopy: The Journal of Arthroscopic & Related Surgery*, 1994, *10*(3), 324–327.

6. Galatz, L. M.; Ball, C. M.; Teefey, S. A.; Middleton, W. D.; Yamaguchi, K. The Outcome and Repair Integrity of Completely Arthroscopically Repaired Large and Massive Rotator Cuff Tears. *J. Bone Joint Surg. Am.*, 2004, *86*(2), 219–224.

7. Rawson, S.; Cartmell, S.; Wong, J. Suture Techniques for Tendon Repair; a Comparative Review. *Muscle Ligaments and Tendons J.*, 2019, *03*(03), 220.

8. Frosch, K.-H.; Preiss, A.; Heider, S.; Stengel, D.; Wohlmuth, P.; Hoffmann, M. F.; Lill, H. Primary Ligament Sutures as a Treatment Option of Knee Dislocations: a Meta-Analysis. *Knee Surg. Sports Traumatol. Arthrosc.*, 2012, *21*(7), 1502–1509.

9. Spalazzi, J. P.; Boskey, A. L.; Pleshko, N.; Lu, H. H. Quantitative Mapping of Matrix Content and Distribution across the Ligament-to-Bone Insertion. *PLOS ONE*, 2013, *8*(9).

10. Olszta, M. J.; Cheng, X.; Jee, S. S.; Kumar, R.; Kim, Y.-Y.; Kaufman, M. J.; Douglas, E. P.; Gower, L. B. Bone Structure and Formation: A New Perspective. *Mat. Sci. Eng. R.*, 2007, *58*(3-5), 77–116.

11. Abraham, A. C.; Donahue, T. L. H. From Meniscus to Bone: A Quantitative Evaluation of Structure and Function of the Human Meniscal Attachments. *Acta Biomater*, 2013, *9*(5), 6322–6329.

12. Moffat, K. L.; Sun, W.-H. S.; Pena, P. E.; Chahine, N. O.; Doty, S. B.; Ateshian, G. A.; Hung, C. T.; Lu, H. H. Characterization of the Structure-Function Relationship at the Ligament-to-Bone Interface. *Proc. Natl. Acad. Sci. U. S. A.*, 2008, *105*(23), 7947–7952.

13. Buckwalter, J. A.; Einhorn, T. A.; Simon, S. R. *Orthopaedic basic science: biology and biomechanics of the musculoskeletal system*; American Academy of Orthopaedic Surgeons: Rosemont, IL, 2000.

14. Smith, L.; Xia, Y.; Galatz, L. M.; Genin, G. M.; Thomopoulos, S. Tissue-Engineering Strategies for the Tendon/Ligament-to-Bone Insertion. *Connective Tissue Res.*, 2011, *53*(2), 95–105.

15. Li, X.; Xie, J.; Lipner, J.; Yuan, X.; Thomopoulos, S.; Xia, Y. Nanofiber Scaffolds with Gradations in Mineral Content for Mimicking the Tendon-to-Bone Insertion Site. *Nano Lett.*, 2009, *9*(7), 2763–2768.

16. Zou, B.; Liu, Y.; Luo, X.; Chen, F.; Guo, X.; Li, X. Electrospun Fibrous Scaffolds with Continuous Gradations in Mineral Contents and Biological Cues for Manipulating Cellular Behaviors. *Acta Biomater,* 2012, *8*(4), 1576–1585.

17. Liu, W.; Lipner, J.; Xie, J.; Manning, C. N.; Thomopoulos, S.; Xia, Y. Nanofiber Scaffolds with Gradients in Mineral Content for Spatial Control of Osteogenesis. *ACS Appl. Mater. Interfaces,* 2014, *6*(4), 2842–2849.

18. Iannucci, L. E.; Boys, A. J.; Mccorry, M. C.; Estroff, L. A.; Bonassar, L. J. Interfaces: Cellular and Chemical Gradients to Engineer the Meniscus-to-Bone Insertion (Adv. Healthcare Mater. 7/2019). *Adv. Healthcare Mater.*, 2019, *8*(7), 1970027.

19. Criscenti, G.; Longoni, A.; Luca, A. D.; Maria, C. D.; Blitterswijk, C. A. V.; Vozzi, G.; Moroni, L. Triphasic Scaffolds for the Regeneration of the Bone–Ligament Interface. *Biofabrication,* 2016, *8*(1), 015009.

20. Spalazzi, J. P.; Doty, S. B.; Moffat, K. L.; Levine, W. N.; Lu, H. H. Development of Controlled Matrix Heterogeneity on a Triphasic Scaffold for Orthopedic Interface Tissue Engineering. *Tissue Eng.*, 2006, 061120052454001.

21. Teh, T. K. H.; Shi, P.; Ren, X.; Hui, J. H. P.; Toh, S. L.; Goh, J. C. H. Ligament-to-Bone Interface Tissue Regeneration Using a Functionalized Biphasic Silk Fibroin Scaffold. *IFMBE Proceedings The 15th International Conference on Biomedical Engineering,* 2014, 64–67.

22. Boys, A. J.; Zhou, H.; Harrod, J. B.; Mccorry, M. C.; Estroff, L. A.; Bonassar, L. J. Top-Down Fabrication of Spatially Controlled Mineral-Gradient Scaffolds for Interfacial Tissue Engineering. *ACS Biomater. Sci. Eng.*, 2019.

23. Gilbert, T.; Sellaro, T.; Badylak, S. Decellularization of Tissues and Organs. *Biomater.*, 2006

24. Papadimitropoulos, A.; Scotti, C.; Bourgine, P.; Scherberich, A.; Martin, I. Engineered Decellularized Matrices to Instruct Bone Regeneration Processes. *Bone,* 2015, *70*, 66–72.

25. Shahab-Osterloh, S.; Witte, F.; Hoffmann, A.; Winkel, A.; Laggies, S.; Neumann, B.; Seiffart, V.; Lindenmaier, W.; Gruber, A. D.; Ringe, J.; Häupl, T.; Thorey, F.; Willbold, E.; Corbeau, P.; Gross, G. Mesenchymal Stem Cell-Dependent Formation of Heterotopic Tendon-Bone Insertions (Osteotendinous Junctions). *Stem Cells*, 2010, 28(9), 1590–1601.

26. Mauney, J. R.; Blumberg, J.; Pirun, M.; Volloch, V.; Vunjak-Novakovic, G.; Kaplan, D. L. Osteogenic Differentiation of Human Bone Marrow Stromal Cells on Partially Demineralized Bone Scaffolds in Vitro. *Tissue Eng.*, 2004, *10*(1-2), 81–92.

27. Ravichandran, R.; Venugopal, J. R.; Sundarrajan, S.; Mukherjee, S.; Ramakrishna, S. Precipitation of Nanohydroxyapatite on PLLA/PBLG/Collagen Nanofibrous Structures for the Differentiation of Adipose Derived Stem Cells to Osteogenic Lineage. *Biomater.*, 2012, *33*(3), 846–855.

28. Wang, Y.; Wu, S.; Kuss, M. A.; Streubel, P. N.; Duan, B. Effects of Hydroxyapatite and Hypoxia on Chondrogenesis and Hypertrophy in 3D Bioprinted ADMSC Laden Constructs. *ACS Biomater. Sci. Eng.*, 2017, 3(5), 826–835.

29. Kuo, Y.-C.; Leou, S.-N. Chondrogenesis of Articular Chondrocytes in Hydroxyapatite/Chitin/Chitosan Scaffolds Supplemented with Pituitary Extract. *Eng. Life Sci.*, 2010, 10(1), 65–74.

30. Spadaccio, C.; Rainer, A.; Trombetta, M.; Vadalá, G.; Chello, M.; Covino, E.; Denaro, V.; Toyoda, Y.; Genovese, J. A. Poly-l-Lactic Acid/Hydroxyapatite Electrospun Nanocomposites Induce Chondrogenic Differentiation of Human MSC. *Ann. Biomed. Eng.*, 2009, *37*(7), 1376–1389.

31. Mccorry, M. C.; Mansfield, M. M.; Sha, X.; Coppola, D. J.; Lee, J. W.; Bonassar, L. J. A Model System for Developing a Tissue Engineered Meniscal Enthesis. *Acta Biomater*, 2017, *56*, 110–117.

32. Ruifrok, A. C. Quantification of histochemical staining by color deconvolution. *Anal. Quant. Cytol. Histol.*, 2001, (0884-6812), 23 (4), p. 291.

33. Varghese, F.; Bukhari, A. B.; Malhotra, R.; De, A. IHC Profiler: An Open Source Plugin for the Quantitative Evaluation and Automated Scoring of Immunohistochemistry Images of Human Tissue Samples. *PLOS ONE*, 2014, *9*(5).

34. Mescher, A. *Junqueiras Basic Histology:12th Revised edition: Text and Atlas*; Mcgraw-hill medical: New york, 2010.

35. Huang, W. Signaling and Transcriptional Regulation in Osteoblast Commitment and Differentiation. *Front. Biosci.*, 2007, 12(8-12), 3068.

36. Ataie, M.; Shabani, I.; Seyedjafari, E. Surface Mineralized Hybrid Nanofibrous Scaffolds Based on Poly(l-Lactide) and Alginate Enhances Osteogenic Differentiation of Stem Cells. *J. Biomed. Mater. Res. A*, 2018, *107*(3), 586–596.

37. Junqueira, L. C.; Bignolas, G.; Brentani, R. R. Picrosirius staining plus polarization microscopy, a specific method for collagen detection in tissue sections. *Histochem. J.* 1979, 11, 447−455.

38. Rich, L.; Whittaker, P. Collagen and Picrosirius Red Staining: a Polarized Light Assessment of Fibrillar Hue and Spatial Distribution. Brazilian *J. Morphol. Sci.* 2005, 22 (2), 97−104.

39. Xu, Y.; James, A. W.; Longaker, M. T. Transforming Growth Factor-β1 Stimulates Chondrogenic Differentiation of Posterofrontal Suture–Derived Mesenchymal Cells In Vitro. *Plast. Reconstr. Surg.*, 2008, 122(6), 1649–1659.

40. Zheng, L.; Yang, J.; Fan, H.; Zhang, X. Material-Induced Chondrogenic Differentiation of Mesenchymal Stem Cells Is Material-Dependent. *Exp. Ther. Med.*, 2014, *7*(5), 1147–1150.

41. Shahmoradi, S. R.; Salmani, M. K.; Soleimanpour, H. R.; Tavakoli, A. H.; Hosaini, K.; Haghighipour, N.; Bonakdar, S. Induction of Chondrogenic Differentiation in Human Mesenchymal Stem Cells Cultured on Human Demineralized Bone Matrix Scaffold under Hydrostatic Pressure. *J. Tissue Eng. Regen. Med.*, 2018, *16*(1), 69–80.

42. Fröhlich, M.; Grayson, W. L.; Marolt, D.; Gimble, J. M.; Kregar-Velikonja, N.; Vunjak-Novakovic, G. Bone Grafts Engineered from Human Adipose-Derived Stem Cells in Perfusion Bioreactor Culture. *Tissue Eng. Part A*, 2010, *16*(1), 179–189.

43. Engineering Anatomically Shaped Human Bone Grafts with Human Mesenchymal Stem Cells (HMSCs). *Science-Business eXchange*, 2009, *2*(41), 1551–1551.

44. Wang, J.; Yang, R.; Gerstenfeld, L. C.; Glimcher, M. J. Characterization of Demineralized Bone Matrix-Induced Osteogenesis in Rat Calvarial Bone Defects: III. Gene and Protein Expression. *Calcif. Tissue Int.*, 2000, *67*(4), 314–320.

45. Grayson, W.; Bhumiratana, S.; Chao, P. G.; Hung, C.; Vunjak-Novakovic, G. Spatial Regulation of Human Mesenchymal Stem Cell Differentiation in Engineered Osteochondral Constructs: Effects of Pre-Differentiation, Soluble Factors and Medium Perfusion. *Osteoarthritis and Cartilage*, 2010, 18(5), 714–723.

46. Cheng, C. W.; Solorio, L. D.; Alsberg, E. Decellularized Tissue and Cell-Derived Extracellular Matrices as Scaffolds for Orthopaedic Tissue Engineering. *Biotechnol. Adv.*, 2014, 32(2), 462–484.

47. Fletcher, J. W. A.; Williams, S.; Whitehouse, M. R.; Gill, H. S.; Preatoni, E. Juvenile Bovine Bone Is an Appropriate Surrogate for Growth and Reduced Density Human Bone in Biomechanical Testing: a Validation Study. *Sci. Rep.*, 2018, *8*(1).

49. Hill, A. B. T.; Bressan, F. F.; Murphy, B. D.; Garcia, J. M. Applications of Mesenchymal Stem Cell Technology in Bovine Species. *Stem Cell Res. Ther.*, 2019, 10(1).

50. Rodríguez-Fuentes, N.; Reynoso-Ducoing, O.; Rodríguez-Hernández, A.; Ambrosio-Hernández, J. R.; Piña-Barba, M. C.; Zepeda-Rodríguez, A.; Cerbón-Cervantes, M. A.; Tapia-Ramírez, J.; Alcantara-Quintana, L. E. Isolation of Human Mesenchymal Stem Cells and Their Cultivation on the Porous Bone Matrix. *J. Vis. Exp.*, 2015, No. 96.

51. Perikamana, S. K. M.; Lee, J.; Park, S. Y.; Jung, H. S.; Shin, H. Effect of Gradient Biomineral Concentrations on Osteogenic and Chondrogenic Differentiation of Adipose Derived Stem Cells. *J. Ind. Eng. Chem.*, 2019.

Chapter 3

Conclusion, Limitations and Future Works

The aim of this thesis was to investigate the MSC behavior controlled by the HAp mineral distribution in a bone scaffold. Spatially controlled osteogenesis by MSCs was observed when the scaffolds were cultured with either growth or osteogenic media. Briefly, MSCs seeded in the mineralized regions of the scaffolds exhibited strong osteogenic commitment while those seeded in the demineralized regions showed delayed appearance of late stage osteogenic biomarker, OCN in growth media. When the seeded scaffolds were cultured with osteogenic media, OCN was expressed in both regions of the scaffolds at early time point. Peak intensity of OCN staining in demineralized regions showed up later than that in mineralized regions, which suggests a delayed process during osteogenic differentiation of MSCs in demineralized regions. The chondrogenesis by MSCs was further investigated when the scaffolds were cultured in a chondrogenic media containing 10ng/mL TGF-β1. Despite MSCs in both regions of the scaffolds initially showed osteogenesis instead of chondrogenesis, the chondrogenic media suppressed the osteogenic biomarkers over time. By day 14, osteogenesis by MSCs in the demineralized regions of the scaffold was completely downregulated by showing negative OCN staining while those in the mineralized regions maintained positive stains of OCN. Our observations on the development of osteogenic biomarkers aligned with previous findings well. Therefore, we conclude that our scaffolds patterned with spatial distribution of HAp are able to control osteogenesis by MSCs.

In addition to controlling osteogenesis by MSCs in our bone scaffold, our scaffolds showed more rapid osteoinductive properties compared to scaffolds studied by other researchers. We observed OCN staining in mineralized region of the scaffold cultured in growth media as

early as day 4 of the culture. In other studies, osteogenic markers usually showed up at day 7 of the culture[1,2,3]. When cultured with osteogenic media, we noticed the condensation of MSCs within the cellular matrix by day 4 of static culture (Fig. 2.3 Column C, highlighted in red circle). These MSC masses were stained heavily by OCN and ALP and resemble the formation of bone blastema[4] (Fig. S2). Our results suggested that the bone scaffolds support accelerated osteogenic differentiation and bone formation *in vitro*. Therefore, we expect our scaffolds to integrate faster at implantation site *in vivo*, which may potentiate shorter time of postoperative recovery for its applications in tissue engineering field.

Several limitations and suggestions for improvement are to be addressed. The histological and IHC analysis was based on visualization of biomarkers of decalcified tissue embedded in paraffin. Some resultant components that are important to further confirm the formation of new mineralized tissue may be removed during the process of decalcification and paraffinization. For example, a standard decalcification procedure requires submerging the tissue in hydrochloric acid, which will dissolve any newly formed HAp by MSCs. Therefore, calcium stains such as alizarin red or von Kossa would not be applicable to those processed tissue. Instead, indirect detection method, such as OCN IHC staining was used to characterize extracellular matrix mineralized by MSCs since OCN protein is associated with the mineralization of matrix. We are also interested in detecting adipogenic cells within the scaffold since they are found in native bone marrow. However, the key biomarker to characterize adipogenic differentiation, lipid will be removed during paraffinization process. We did not find a substitutional biomarker to indirectly detect lipid formation. Future experiments may utilize different embedding technique such as optimal cutting temperature (OCT) compound or agarose to preserve the mineral and lipid possibly formed in our cultured scaffold.

In future experiments, we will apply the MSC-seeded bone plugs in a full tissue engineered meniscus construct cultured in the diffusion chamber bioreactor with media gradients. Several recommendations of changes can be made to the current existing protocol based on the findings of this thesis. Choices of media are important to exert control over differentiation of MSCs. We have shown that in growth media, MSCs in the mineralized regions of the scaffolds exhibited osteogenesis while those in the demineralized regions of the scaffolds showed delayed appearance of osteogenic markers at day 4 of the static culture. In contrast, MSCs cultured in osteogenic media showed global osteogenesis within the scaffold. Therefore, growth media may be more suitable during seeding process to keep MSCs in the demineralized regions of the scaffolds from overcommitting osteogenic differentiation. Following the seeding process, the demineralized side of the MSC-seeded scaffold will be injected with collagen gel seeded with fibrocartilage chondrocytes. The entire construct will be cultured in the diffusion chamber bioreactor. The collagen gel and the demineralized bone conjunction will be supplied with chondrogenic media containing TGF-β1. This chondrogenic cocktail is supposed to improve fiber formation and alignment of fibrocartilage chondrocytes in collagen gel and chondrogenic differentiation of MSCs. However, it should be noticed that the chondrogenic media will affect the biochemical environment in the mineralized regions of the scaffold since the bioreactor introduce media gradient along the bone scaffold. This chondrogenic biochemical environment can suppress osteoinducing property and change cellular phenotype in the mineralized regions of the scaffolds based on our observation. Therefore, an osteogenic media may be more suitable for filling in the chamber to culture MSCs in the mineralized regions of the scaffolds. Meanwhile, a complete osteogenic media containing dexamesathone, ascorbic acid and β-glycerophosphate will also affect MSCs in the demineralized regions of the scaffold.

Therefore, it may be worthy experimenting with a less strong osteogenic media containing any two of the osteogenic components.

The results from this thesis contribute to better understandings of MSC behaviors on the bone scaffold containing mineral gradient developed in our lab. They also laid down framework to create a tissue engineered meniscal enthesis, potentially with better biomimicry to native cellular complexity and improved integration between hard and soft tissues.

Reference

1. Zou, B.; Liu, Y.; Luo, X.; Chen, F.; Guo, X.; Li, X. Electrospun Fibrous Scaffolds with Continuous Gradations in Mineral Contents and Biological Cues for Manipulating Cellular Behaviors. *Acta Biomater*, 2012, *8*(4), 1576–1585.

2. Liu, W.; Lipner, J.; Xie, J.; Manning, C. N.; Thomopoulos, S.; Xia, Y. Nanofiber Scaffolds with Gradients in Mineral Content for Spatial Control of Osteogenesis. *ACS Appl. Mater. Interfaces*, 2014, *6*(4), 2842–2849.

3. 51. Perikamana, S. K. M.; Lee, J.; Park, S. Y.; Jung, H. S.; Shin, H. Effect of Gradient Biomineral Concentrations on Osteogenic and Chondrogenic Differentiation of Adipose Derived Stem Cells. *J. Ind. Eng. Chem.*, 2019.

4. Mescher, A. *Junqueiras Basic Histology:12th Revised edition: Text and Atlas*; Mcgraw-hill medical: New york, 2010.

Appendix 1: Supplemental Figures

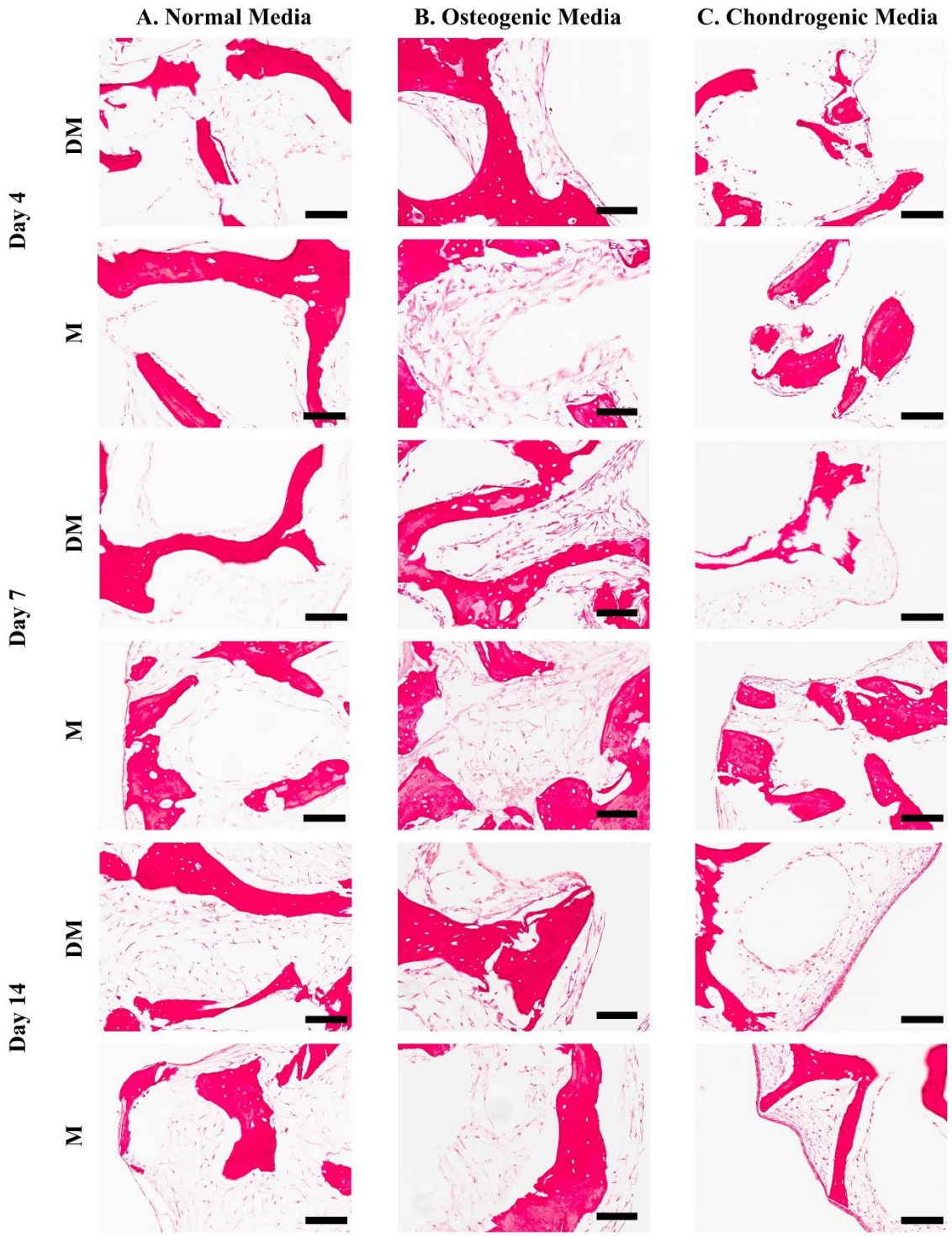

S1. Unpolarized images of seeded scaffolds stained by Picrosirius Red corresponding to static culture in Column A) growth media, Column B) osteogenic media, Column C) chondrogenic media. Scale bars are 100 µm.

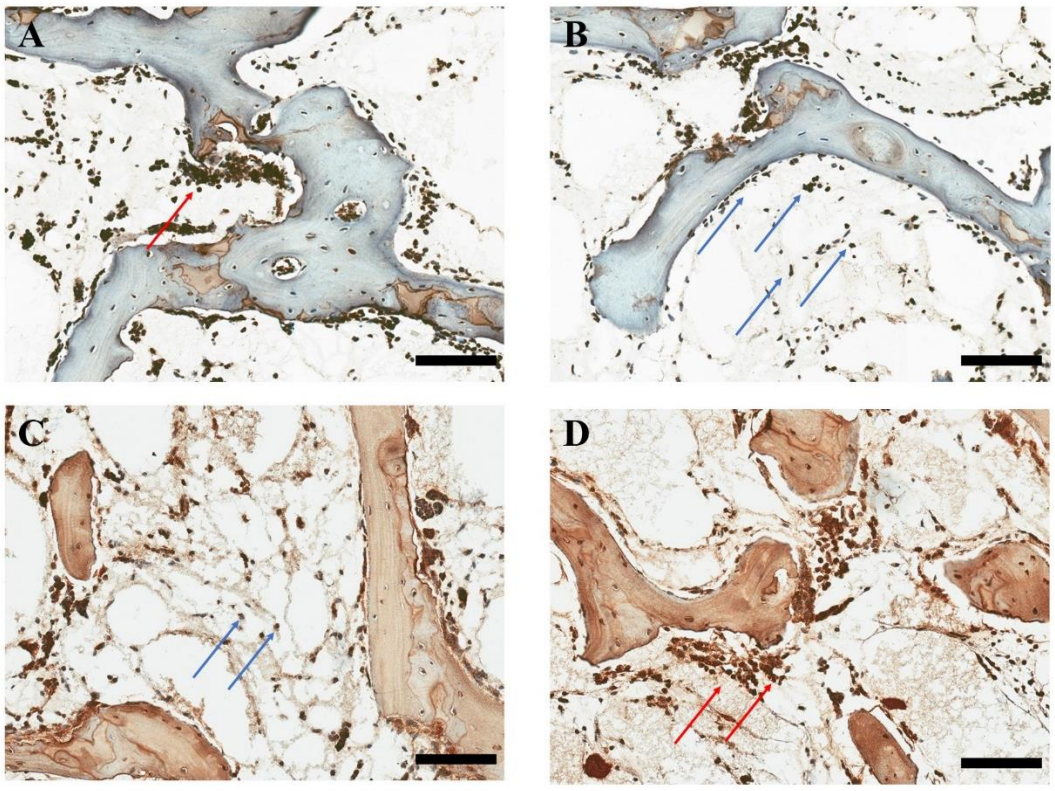

S2. IHC stains on native trabecular tissue. A) and B) Active osteoblasts were stained positive in ALP as indicated by red arrows. Mature osteoblasts were stained negative in ALP as indicated by blue arrows. C) and D) Mature osteoblasts has limited stain of OCN as indicated by blue arrows. Active osteoblasts showed strong OCN stain as indicated by red arrows. Cell masses showed in A) and D) may indicate direct formation of new trabecular bone. Scale bars are 100 µm.

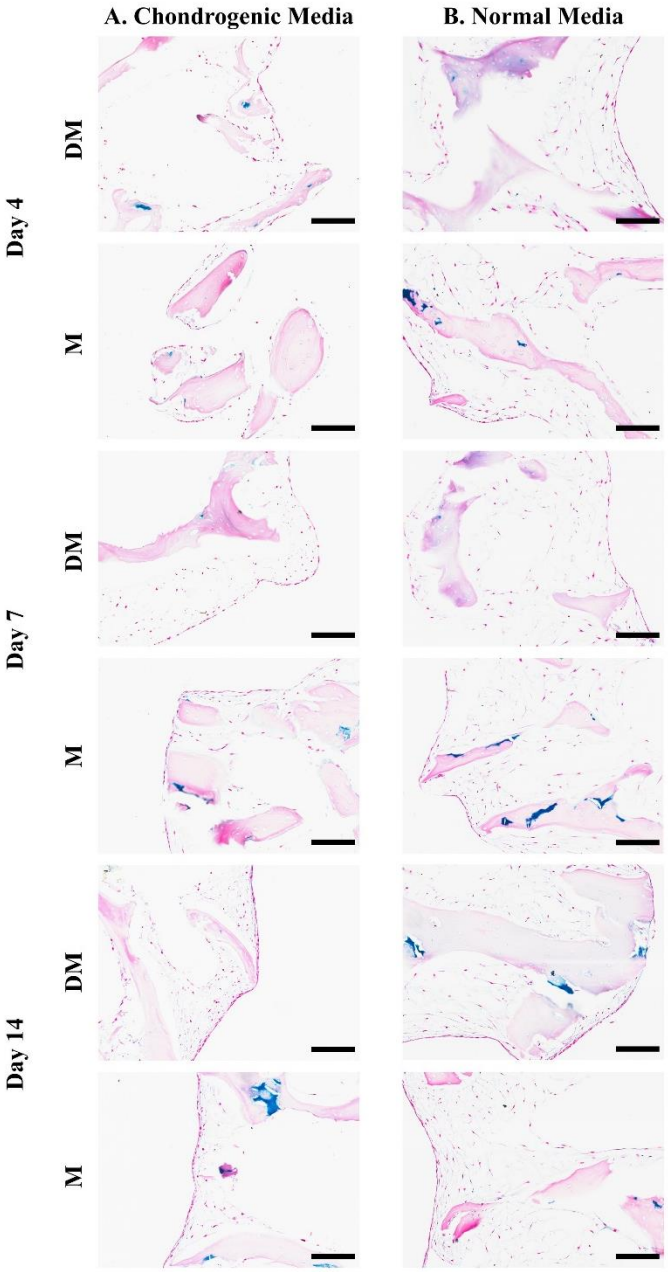

S3. Alcian blue stain on seeded scaffolds cultured with Column A) chondrogenic media and Column B) growth media. Scale bars=100 µm.

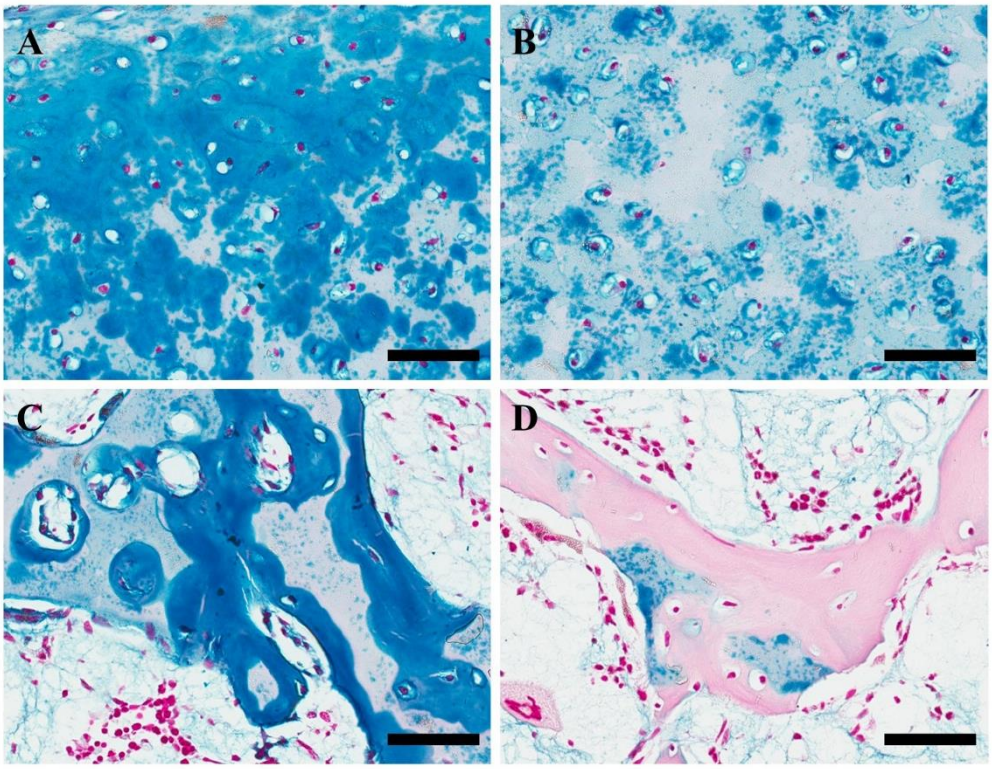

S4. Alcian blue score of native neonatal bovine patella osteochondral interface was evaluated in different regions. A) Articular cartilage scored 3.29. B) Deep zone cartilage scored 2.04. C) Interface scored 2.84. D) Trabecular bone scored 1.41. Scale bars are 50 µm.

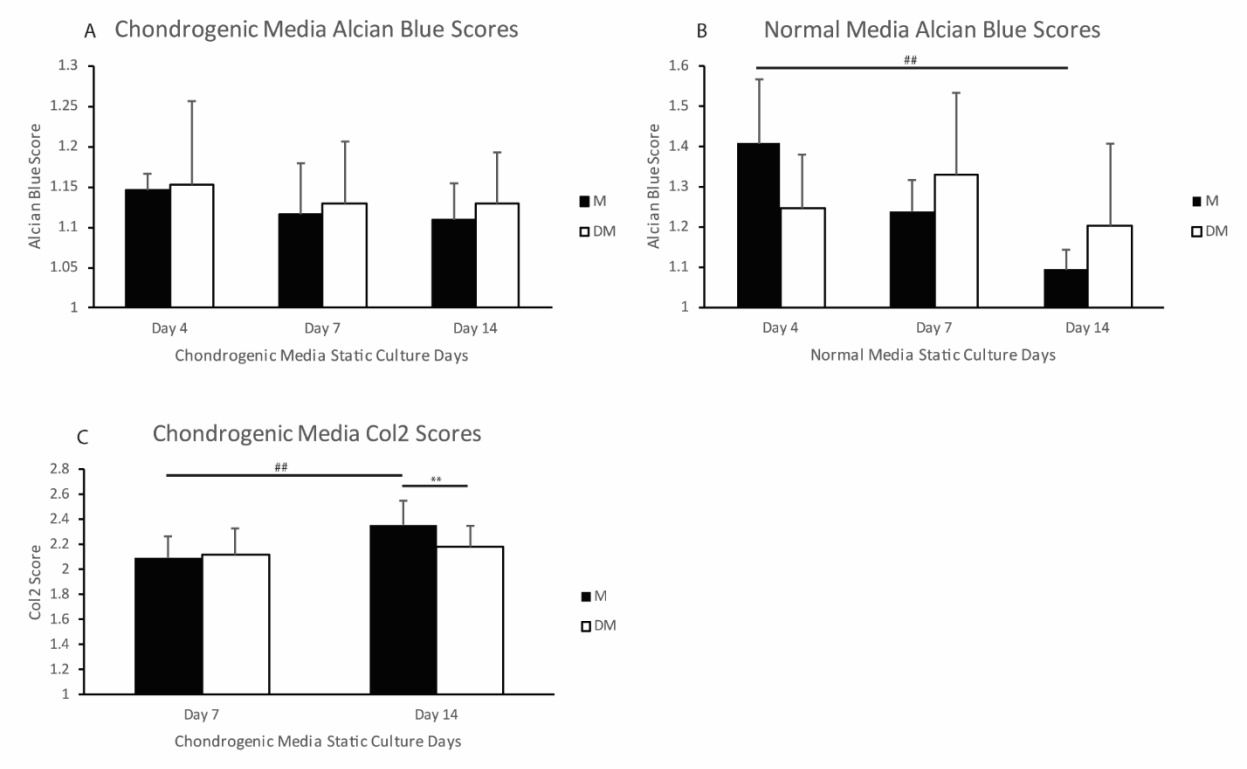

S5. A) and B) are Alcian blue scores of seeded scaffolds quantified by ImageJ. No significant difference was observed between chondrogenic group and growth group. Scores were not comparable to values from native cartilage nor bone tissue. C) is the Col II scores of seeded scaffolds quantified by ImageJ.

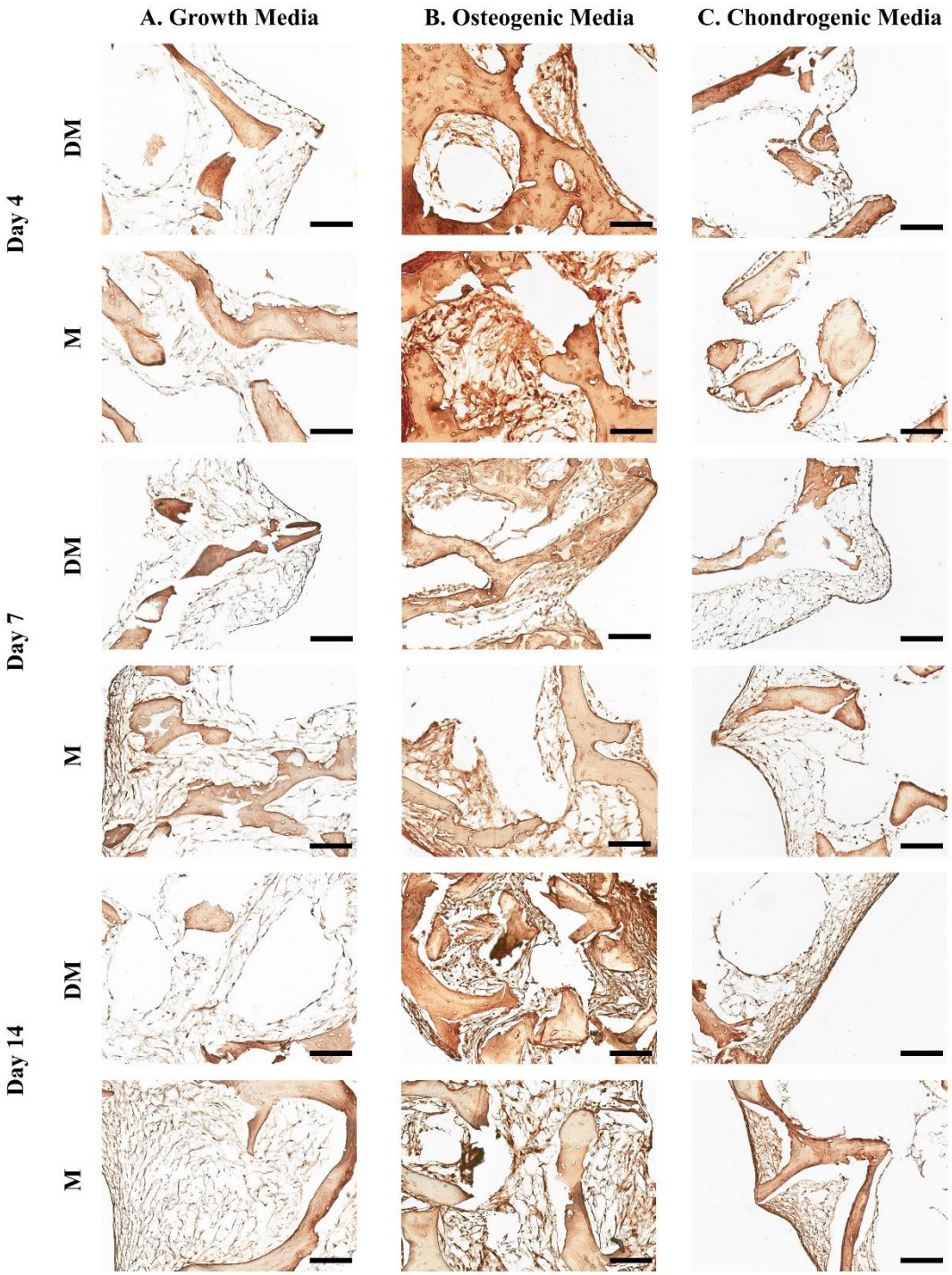

S6. Col I IHC stains on seeded scaffolds cultured with Column A) chondrogenic media and Column B) growth media. Scale bars are 100 µm.

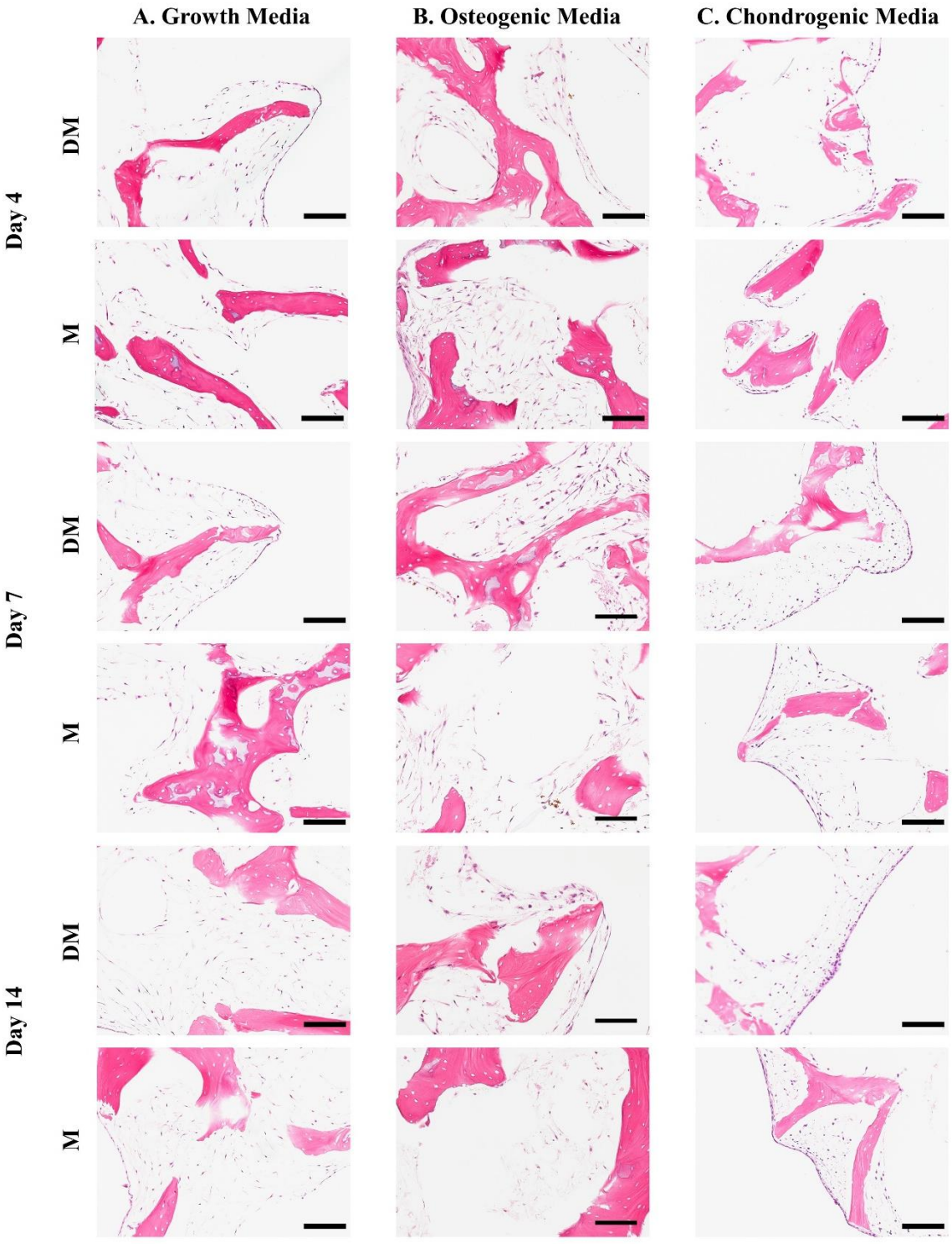

S7. H&E stains on seeded scaffolds cultured with Column A) growth media, Column B) osteogenic media and Column C) chondrogenic media. Scale bars are 100 µm.

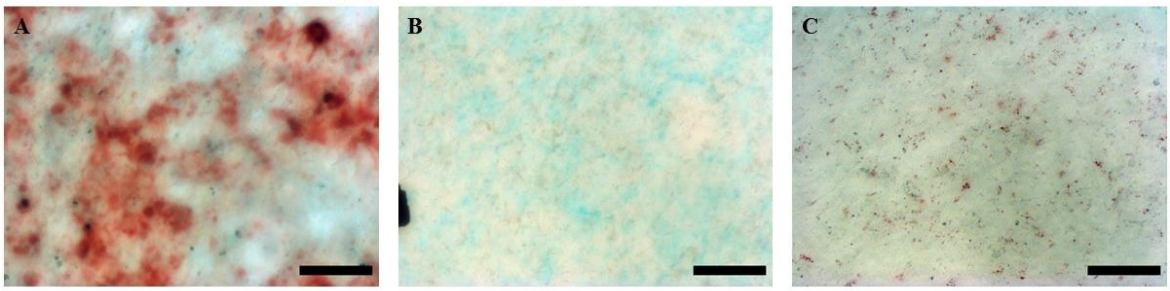

S8. Mesenchymal stem cells triple lineage test. A) MSCs cultured in osteogenic media stained by Alizarin red showed positive staining of minerals (red). B) MSCs cultured in chondrogenic media stained by Alcian blue showed positive staining of GAGs (blue). C) MSCs cultured in adipogenic media stained by Oil red O showed positive staining of lipids (red). Scale bars are 100 µm.

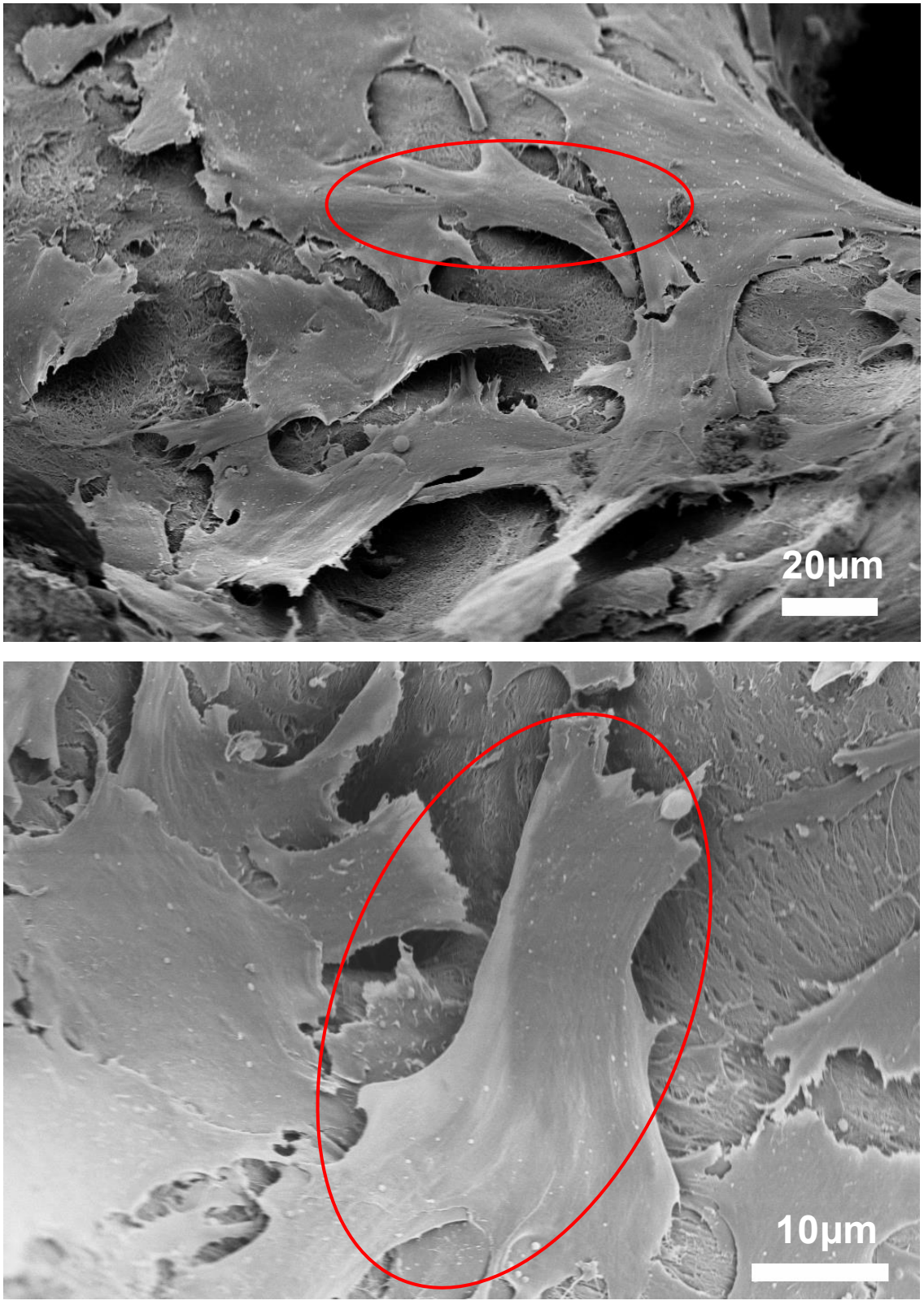

S9. Initial MSC attachment on the bone scaffolds cultured in osteogenic media by day 4 acquired by LEO 1550 FESEM. Cells highlighted by red circles.

Appendix 2: Statistical Analysis

Data Normality Test

ANOVA test and Tukey's post-hoc test was conducted using R studio software. This supplementary data shows the codes to run statistical analysis in R.

ANOVA test and Tukey's post-hoc test within OCN Scores:

```
library(lmerTest)
library(ggplot2)
library(PMCMR)
library(dunn.test)
library(lme4)
library(lsmeans)
library(car)
library(multcomp)
library(pwr)
library(simr)
#read in csv data

full = read.csv("C:\\Users\\James Zhou\\Desktop\\IHC  Scoring Statistics for R\\OCN_CSV.csv")
summary(full)

#change Media and MD to categorical variables
full$Media  = as.factor(full$Media)
full$M.or.D  = as.factor(full$M.or.D)

#first make histograms of each of the response variables
hist(full$OCN.Score, breaks = 20)

#now plot each of the response variables versus each predictor
#OCN.Score
boxplot(full$OCN.Score  ~ full$Media, main = "Media")
boxplot(full$OCN.Score  ~ full$M.or.D, main = "M.or.D")
boxplot(full$OCN.Score  ~ full$Time, main = "Time")
```

```
#now run a lm (linear model) on constructs for each input variable and see the results
fMedia = lm((OCN.Score) ~ Media, data = full)
fM.or.D = lm ((OCN.Score) ~ M.or.D, data = full)
fTime = lm((OCN.Score) ~ Time, data = full)

model = lm(OCN.Score ~ Media + M.or.D  + Time, data = full)

#check these plots for growthity
qqPlot(resid(fMedia))  #if dots are not within red dashed lines then try to log transform or sqrt your output data.
qqPlot(resid(fM.or.D))
qqPlot(resid(fTime))

plot(residuals(fMedia) ~ predict(fMedia)) # are your dots randomLy distributed around zero if not try to log or sqrt your output data and run the model again
plot(residuals(fM.or.D) ~ predict(fM.or.D))
plot(residuals(fTime) ~ predict(fTime))

anova(fMedia)
anova(fM.or.D)
anova(fTime)

lsmeans(fMedia, pairwise~Media)
lsmeans(fM.or.D, pairwise~M.or.D)
lsmeans(fTime, pairwise~Time)

fMedia3 = kruskal.test(OCN.Score ~ Media, data = full)
posthoc.kruskal.dunn.test(x = full$OCN.Score, g = full$Media, p.adjust.method = "bonferroni")
fM.or.D3 = kruskal.test(OCN.Score ~ M.or.D, data = full)
posthoc.kruskal.dunn.test(x = full$OCN.Score, g = full$M.or.D, p.adjust.method = "bonferroni")
fTime3 = kruskal.test(OCN.Score ~ Time, data = full)
posthoc.kruskal.dunn.test(x = full$OCN.Score, g = full$Time, p.adjust.method = "bonferroni")
```

Results showed within different media supplement, there was significant difference between media O and media C (1.8e-9), Media O and Media N (1.6e-12). Within different

mineralization states, there was significant difference between M and D (p=1.6e-14). Within different time points, there was significant difference between 4 and 14 days (p=5.8e-5).

ANOVA test and Tukey's post-hoc test within ALP Scores:

```
setwd("C:\Users\James Zhou\Desktop\IHC Scoring Statistics for R\ALP CSV.csv')
library(lmerTest)
library(ggplot2)
library(PMCMR)
library(dunn.test)
library(lme4)
library(lsmeans)
library(car)
library(multcomp)
library(pwr)
library(simr)
library(Surrogate)
#read in csv data

full = read.csv("C:\\Users\\James Zhou\\Desktop\\IHC Scoring Statistics for R\\ALP CSV.csv")
summary(full)

#change Media and MD to categorical variables
full$Media = as.factor(full$Media)
full$M.or.D = as.factor(full$M.or.D)

#first make histograms of each of the response variables
hist(full$ALP.Score, breaks = 20)

#now plot each of the response variables versus each predictor
#ALP.Score
boxplot(full$ALP.Score ~ full$Media, main = "Media")
boxplot(full$ALP.Score ~ full$M.or.D, main = "M.or.D")
boxplot(full$ALP.Score ~ full$Time, main = "Time")

#now run a lm (linear model) on constructs for each input variable and see the results
fMedia = lm((OCN.Score) ~ Media, data = full)
fM.or.D = lm ((OCN.Score) ~ M.or.D, data = full)
```

```
fTime = lm((OCN.Score) ~ Time, data = full)

model = lm(ALP.Score ~ Media + M.or.D + Time, data = full)

#check these plots for growthity
qqPlot(resid(fMedia))  #if dots are not within red dashed lines then try to log transform or sqrt your output data.
qqPlot(resid(fM.or.D))
qqPlot(resid(fTime))

plot(residuals(fMedia) ~ predict(fMedia)) # are your dots randomLy distributed around zero if not try to log or sqrt your output data and run the model again
plot(residuals(fM.or.D) ~ predict(fM.or.D))
plot(residuals(fTime) ~ predict(fTime))

anova(fMedia)
anova(fM.or.D)
anova(fTime)

lsmeans(fMedia, pairwise~Media)
lsmeans(fM.or.D, pairwise~M.or.D)
lsmeans(fTime, pairwise~Time)

fMedia3 = kruskal.test(ALP.Score ~ Media, data = full)
posthoc.kruskal.dunn.test(x = full$ALP.Score, g = full$Media, p.adjust.method = "bonferroni")
fM.or.D3 = kruskal.test(ALP.Score ~ M.or.D, data = full)
posthoc.kruskal.dunn.test(x = full$ALP.Score, g = full$M.or.D, p.adjust.method = "bonferroni")
fTime3 = kruskal.test(ALP.Score ~ Time, data = full)
posthoc.kruskal.dunn.test(x = full$ALP.Score, g = full$Time, p.adjust.method = "bonferroni")
```

Results showed within different media supplement, there was significant difference between media N and media C (0.0027), Media O and Media N (7e-05). Within different time points, there was significant difference between 4 and 14 days (p=2e-16), 4 and 7 days (p=5.7e-16) and 7 and 14 days (p=1.6e-9).

Tukey HSD Pairwise Test

Pairwise comparisons in single media treatment group was conducted using R. Report shows the significance of difference between each pair. Each sample is designated as "media treatment-day of culture-mineralization condition".

OCN Scores Osteogenic Media

```
data1 <- read.table("OOCN.txt",header=T)
amod1 <- aov(OCN_Score~Sample,data=data1)
summary(amod1)
```

```
##              Df Sum Sq Mean Sq F value   Pr(>F)
## Sample        5  3.443  0.6885   9.331 1.79e-07 ***
## Residuals   114  8.412  0.0738
## ---
## Signif. codes:  0 '***' 0.001 '**' 0.01 '*' 0.05 '.' 0.1 ' ' 1
```

```
tmod1 <- glht(amod1,linfct=mcp(Sample="Tukey"))
summary(tmod1)
```

```
##
##   Simultaneous Tests for General Linear Hypotheses
##
## Multiple Comparisons of Means: Tukey Contrasts
##
##
## Fit: aov(formula = OCN_Score ~ Sample, data = data1)
##
## Linear Hypotheses:
##                   Estimate Std. Error t value Pr(>|t|)
## O14M - O14D == 0  0.14997    0.08590   1.746  0.50474
## O4D - O14D == 0   0.19526    0.08590   2.273  0.21365
## O4M - O14D == 0   0.49942    0.08590   5.814  < 0.001 ***
## O7D - O14D == 0   0.40706    0.08590   4.739  < 0.001 ***
## O7M - O14D == 0   0.35854    0.08590   4.174  < 0.001 ***
## O4D - O14M == 0   0.04529    0.08590   0.527  0.99497
## O4M - O14M == 0   0.34945    0.08590   4.068  0.00124 **
## O7D - O14M == 0   0.25709    0.08590   2.993  0.03888 *
## O7M - O14M == 0   0.20858    0.08590   2.428  0.15532
## O4M - O4D == 0    0.30416    0.08590   3.541  0.00743 **
## O7D - O4D == 0    0.21179    0.08590   2.466  0.14340
## O7M - O4D == 0    0.16328    0.08590   1.901  0.40690
## O7D - O4M == 0   -0.09236    0.08590  -1.075  0.89024
## O7M - O4M == 0   -0.14087    0.08590  -1.640  0.57406
## O7M - O7D == 0   -0.04851    0.08590  -0.565  0.99308
## ---
## Signif. codes:  0 '***' 0.001 '**' 0.01 '*' 0.05 '.' 0.1 ' ' 1
## (Adjusted p values reported -- single-step method)
```

ALP Scores Osteogenic Media

```
data2 <- read.table("OALP.txt",header=T)
amod2 <- aov(ALP_Score~Sample,data=data2)
summary(amod2)
```

```
##              Df Sum Sq Mean Sq F value Pr(>F)
## Sample        5 26.244   5.249   106.6 <2e-16 ***
## Residuals   114  5.611   0.049
## ---
## Signif. codes:  0 '***' 0.001 '**' 0.01 '*' 0.05 '.' 0.1 ' ' 1
```

```
tmod2 <- glht(amod2,linfct=mcp(Sample="Tukey"))
summary(tmod2)
```

```
##
##   Simultaneous Tests for General Linear Hypotheses
##
## Multiple Comparisons of Means: Tukey Contrasts
##
##
## Fit: aov(formula = ALP_Score ~ Sample, data = data2)
##
## Linear Hypotheses:
##                   Estimate Std. Error t value Pr(>|t|)
## O14M - O14D == 0 -0.04783    0.07015  -0.682    0.984
## O4D - O14D == 0   1.13592    0.07015  16.192   <0.001 ***
## O4M - O14D == 0   1.07415    0.07015  15.311   <0.001 ***
## O7D - O14D == 0   0.74745    0.07015  10.654   <0.001 ***
## O7M - O14D == 0   0.56128    0.07015   8.001   <0.001 ***
## O4D - O14M == 0   1.18375    0.07015  16.873   <0.001 ***
## O4M - O14M == 0   1.12198    0.07015  15.993   <0.001 ***
## O7D - O14M == 0   0.79528    0.07015  11.336   <0.001 ***
## O7M - O14M == 0   0.60911    0.07015   8.682   <0.001 ***
## O4M - O4D == 0   -0.06176    0.07015  -0.880    0.950
## O7D - O4D == 0   -0.38847    0.07015  -5.537   <0.001 ***
## O7M - O4D == 0   -0.57464    0.07015  -8.191   <0.001 ***
## O7D - O4M == 0   -0.32670    0.07015  -4.657   <0.001 ***
## O7M - O4M == 0   -0.51288    0.07015  -7.311   <0.001 ***
## O7M - O7D == 0   -0.18617    0.07015  -2.654    0.093 .
## ---
## Signif. codes:  0 '***' 0.001 '**' 0.01 '*' 0.05 '.' 0.1 ' ' 1
## (Adjusted p values reported -- single-step method)
```

OCN Scores Normal Media

```
data3 <- read.table("NOCN.txt",header=T)
amod3 <- aov(OCN_Score~Sample,data=data3)
summary(amod3)
```

```
##              Df Sum Sq Mean Sq F value Pr(>F)
## Sample        5  14.09  2.8185   49.66 <2e-16 ***
## Residuals   114   6.47  0.0568
```

```
## ---
## Signif. codes:  0 '***' 0.001 '**' 0.01 '*' 0.05 '.' 0.1 ' ' 1
```

```
tmod3 <- glht(amod3,linfct=mcp(Sample="Tukey"))
summary(tmod3)
```

```
##
##   Simultaneous Tests for General Linear Hypotheses
##
## Multiple Comparisons of Means: Tukey Contrasts
##
##
## Fit: aov(formula = OCN_Score ~ Sample, data = data3)
##
## Linear Hypotheses:
##                   Estimate Std. Error t value Pr(>|t|)
## N14M - N14D == 0  0.30366    0.07534   4.031  0.00138 **
## N4D - N14D == 0  -0.73018    0.07534  -9.692  < 0.001 ***
## N4M - N14D == 0   0.22012    0.07534   2.922  0.04714 *
## N7D - N14D == 0  -0.14871    0.07534  -1.974  0.36373
## N7M - N14D == 0   0.13072    0.07534   1.735  0.51180
## N4D - N14M == 0  -1.03384    0.07534 -13.723  < 0.001 ***
## N4M - N14M == 0  -0.08354    0.07534  -1.109  0.87682
## N7D - N14M == 0  -0.45238    0.07534  -6.005  < 0.001 ***
## N7M - N14M == 0  -0.17295    0.07534  -2.296  0.20439
## N4M - N4D == 0    0.95030    0.07534  12.614  < 0.001 ***
## N7D - N4D == 0    0.58146    0.07534   7.718  < 0.001 ***
## N7M - N4D == 0    0.86089    0.07534  11.427  < 0.001 ***
## N7D - N4M == 0   -0.36884    0.07534  -4.896  < 0.001 ***
## N7M - N4M == 0   -0.08941    0.07534  -1.187  0.84233
## N7M - N7D == 0    0.27943    0.07534   3.709  0.00424 **
## ---
## Signif. codes:  0 '***' 0.001 '**' 0.01 '*' 0.05 '.' 0.1 ' ' 1
## (Adjusted p values reported -- single-step method)
```

ALP Scores Normal Media

```
data4 <- read.table("NALP.txt",header=T)
amod4 <- aov(ALP_Score~Sample,data=data4)
summary(amod4)
```

```
##              Df Sum Sq Mean Sq F value   Pr(>F)
## Sample        5  1.898  0.3797   8.422 8.29e-07 ***
## Residuals   114  5.139  0.0451
## ---
## Signif. codes:  0 '***' 0.001 '**' 0.01 '*' 0.05 '.' 0.1 ' ' 1
```

```
tmod4 <- glht(amod4,linfct=mcp(Sample="Tukey"))
summary(tmod4)
```

```
##
##   Simultaneous Tests for General Linear Hypotheses
##
## Multiple Comparisons of Means: Tukey Contrasts
##
##
## Fit: aov(formula = ALP_Score ~ Sample, data = data4)
##
## Linear Hypotheses:
##                   Estimate Std. Error t value Pr(>|t|)
## N14M - N14D == 0 -0.14808    0.06714  -2.205  0.24344
## N4D - N14D == 0   0.03510    0.06714   0.523  0.99517
## N4M - N14D == 0   0.23043    0.06714   3.432  0.01046 *
## N7D - N14D == 0   0.08688    0.06714   1.294  0.78774
## N7M - N14D == 0   0.19369    0.06714   2.885  0.05199 .
## N4D - N14M == 0   0.18318    0.06714   2.728  0.07765 .
## N4M - N14M == 0   0.37851    0.06714   5.638  < 0.001 ***
## N7D - N14M == 0   0.23496    0.06714   3.499  0.00851 **
## N7M - N14M == 0   0.34177    0.06714   5.090  < 0.001 ***
## N4M - N4D == 0    0.19533    0.06714   2.909  0.04853 *
## N7D - N4D == 0    0.05178    0.06714   0.771  0.97181
## N7M - N4D == 0    0.15859    0.06714   2.362  0.17871
## N7D - N4M == 0   -0.14355    0.06714  -2.138  0.27541
## N7M - N4M == 0   -0.03674    0.06714  -0.547  0.99402
## N7M - N7D == 0    0.10681    0.06714   1.591  0.60633
## ---
## Signif. codes:  0 '***' 0.001 '**' 0.01 '*' 0.05 '.' 0.1 ' ' 1
## (Adjusted p values reported -- single-step method)
```

OCN Scores Chondrogenic Media

```
data5 <- read.table("COCN.txt",header=T)
amod5 <- aov(OCN_Score~Sample,data=data5)
summary(amod5)

##              Df Sum Sq Mean Sq F value Pr(>F)
## Sample        5  8.904  1.7808    33.4 <2e-16 ***
## Residuals   114  6.078  0.0533
## ---
## Signif. codes:  0 '***' 0.001 '**' 0.01 '*' 0.05 '.' 0.1 ' ' 1

tmod5 <- glht(amod5,linfct=mcp(Sample="Tukey"))
summary(tmod5)

##
##   Simultaneous Tests for General Linear Hypotheses
##
## Multiple Comparisons of Means: Tukey Contrasts
##
##
## Fit: aov(formula = OCN_Score ~ Sample, data = data5)
```

```
##
## Linear Hypotheses:
##                   Estimate Std. Error t value Pr(>|t|)
## C14M - C14D == 0  0.40230    0.07302   5.509  < 0.001 ***
## C4D - C14D == 0   0.60566    0.07302   8.294  < 0.001 ***
## C4M - C14D == 0   0.84773    0.07302  11.610  < 0.001 ***
## C7D - C14D == 0   0.19821    0.07302   2.714  0.08015 .
## C7M - C14D == 0   0.46319    0.07302   6.343  < 0.001 ***
## C4D - C14M == 0   0.20337    0.07302   2.785  0.06716 .
## C4M - C14M == 0   0.44544    0.07302   6.100  < 0.001 ***
## C7D - C14M == 0  -0.20409    0.07302  -2.795  0.06557 .
## C7M - C14M == 0   0.06089    0.07302   0.834  0.96058
## C4M - C4D == 0    0.24207    0.07302   3.315  0.01521 *
## C7D - C4D == 0   -0.40745    0.07302  -5.580  < 0.001 ***
## C7M - C4D == 0   -0.14248    0.07302  -1.951  0.37699
## C7D - C4M == 0   -0.64953    0.07302  -8.895  < 0.001 ***
## C7M - C4M == 0   -0.38455    0.07302  -5.266  < 0.001 ***
## C7M - C7D == 0    0.26498    0.07302   3.629  0.00551 **
## ---
## Signif. codes:  0 '***' 0.001 '**' 0.01 '*' 0.05 '.' 0.1 ' ' 1
## (Adjusted p values reported -- single-step method)
```

ALP Scores Chondrogenic Media

```
data6 <- read.table("CALP.txt",header=T)
amod6 <- aov(ALP_Score~Sample,data=data6)
summary(amod6)
```

```
##              Df Sum Sq Mean Sq F value  Pr(>F)
## Sample        5  2.842  0.5683   10.06 5.4e-08 ***
## Residuals   114  6.442  0.0565
## ---
## Signif. codes:  0 '***' 0.001 '**' 0.01 '*' 0.05 '.' 0.1 ' ' 1
```

```
tmod6 <- glht(amod6,linfct=mcp(Sample="Tukey"))
summary(tmod6)
```

```
##
##   Simultaneous Tests for General Linear Hypotheses
##
## Multiple Comparisons of Means: Tukey Contrasts
##
##
## Fit: aov(formula = ALP_Score ~ Sample, data = data6)
##
## Linear Hypotheses:
##                    Estimate Std. Error t value Pr(>|t|)
## C14M - C14D == 0 -0.166235   0.075173  -2.211  0.24062
## C4D - C14D == 0   0.299377   0.075173   3.983  0.00171 **
## C4M - C14D == 0   0.209405   0.075173   2.786  0.06716 .
## C7D - C14D == 0  -0.006755   0.075173  -0.090  1.00000
```

```
## C7M - C14D == 0   0.131790   0.075173   1.753  0.50003
## C4D - C14M == 0   0.465612   0.075173   6.194  < 0.001 ***
## C4M - C14M == 0   0.375640   0.075173   4.997  < 0.001 ***
## C7D - C14M == 0   0.159480   0.075173   2.122  0.28377
## C7M - C14M == 0   0.298025   0.075173   3.965  0.00171 **
## C4M - C4D == 0   -0.089972   0.075173  -1.197  0.83753
## C7D - C4D == 0   -0.306132   0.075173  -4.072  0.00120 **
## C7M - C4D == 0   -0.167587   0.075173  -2.229  0.23258
## C7D - C4M == 0   -0.216160   0.075173  -2.876  0.05332 .
## C7M - C4M == 0   -0.077615   0.075173  -1.032  0.90602
## C7M - C7D == 0    0.138545   0.075173   1.843  0.44252
## ---
## Signif. codes:  0 '***' 0.001 '**' 0.01 '*' 0.05 '.' 0.1 ' ' 1
## (Adjusted p values reported -- single-step method)
```

Appendix 3: ImageJ Macro

1. ImageJ Macro to Quantify DAB Stain

A macro in ImageJ was used to split images of DAB stain from the counterstain of hematoxylin and return predefined 8-bit images of only DAB. The threshold was determined from DAB stain of native patella osteochondral interface.

For measurements, an IHC image was loaded in ImageJ.

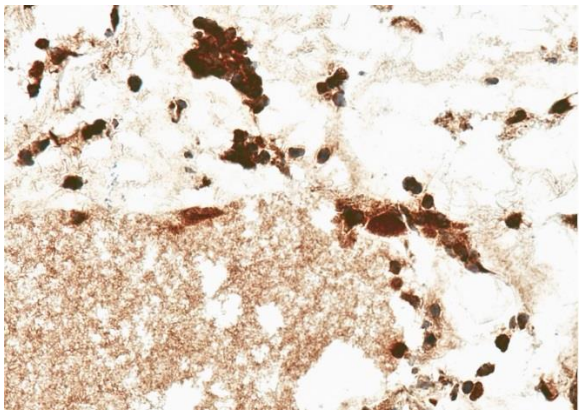

Then, the following code will split the channels:

```
run("Colour Deconvolution", "vectors=[User values] [r1]=39.978916 [g1]=44.231213 [b1]=43.2917 [r2]=11.444741 [g2]=35.436684 [b2]=52.491734 [r3]=0.3044114 [g3]=0.16826215 [b3]=0.291805");
```

This code returns three images of only hematoxylin, DAB and residue.

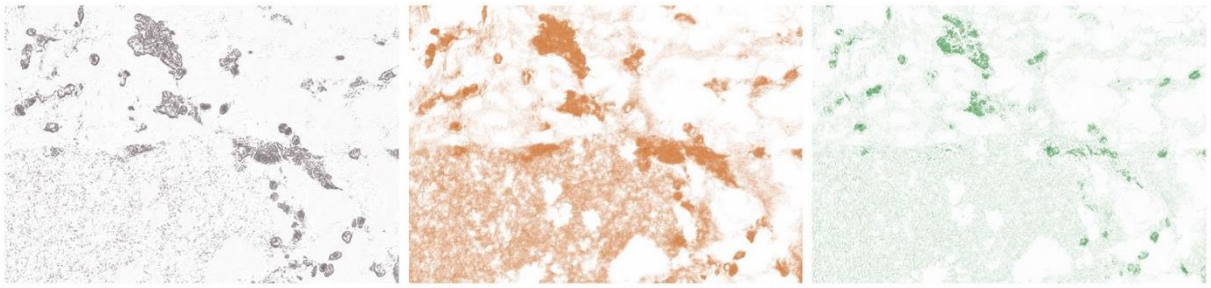

Hematoxylin (Channel 1) DAB (Channel 2) Residual image (Channel 3)

After that, channel 2 which only contains DAB stain in 8 bit was analyze by a macro in the plugin of IHC profiler using the following code:

```
bins = 256;
 maxCount = 0;
 histMin = 0;
 histMax = 0;
 if (histMax>0)
        getHistogram(values, counts, bins, histMin, histMax);
```

```
else
        getHistogram(values, counts, bins);
is8bits = bitDepth()==8 || bitDepth()==24;
Plot.create("Histogram", "Pixel Value", "Count", values, counts);
if (maxCount>0)
        Plot.setLimits(0, 256, 0, maxCount);
n = 0;
sum = 0;
min = 9999999;
max = -9999999;
Region2=0;
Region3=0;
Region4=0;
Region1=0;
Region0=0;
TotalPixel=0;
PercentRegion1=0;
PercentRegion2=0;
PercentRegion4=0;
PercentRegion3=0;
PercentRegion0=0;
Score=0;
PixelUnderConsideration=0;
for (i=0; i<bins; i++)
        {
    count = counts[i];
    if (count>0)
                {
         n += count;
         sum += count*i;
         if (i<min) min = i;
         if (i>max) max = i;
        }
        }
var x=0.025, y=0.1; // global variables
print("Pixel Count: "+n);
if (is8bits)
        {
```

```
                for (i=0; i<bins; i++)
                        {
                    if (i>=0 && i<61)
                            Region4=Region4+counts[i];
                        if (i>60 && i<121)
                    Region3=Region3+counts[i];
                        if (i>120 && i<181)
                    Region2=Region2+counts[i];
                        if (i>180 && i<236)
                    Region1=Region1+counts[i];
                if (i>235 && i<=256)
                    Region0=Region0+counts[i];
                        }
                }
        function draw(text)
                {
                 Plot.addText(text, x, y);
            y += 0.08;
                }
        TotalPixel=TotalPixel+Region1+Region2+Region3+Region4+Region0;
        PixelUnderConsideration=TotalPixel-Region0;
        PercentRegion3=(Region3/PixelUnderConsideration)*100;
        PercentRegion2=(Region2/PixelUnderConsideration)*100;
        PercentRegion1=(Region1/PixelUnderConsideration)*100;
        PercentRegion4=(Region4/PixelUnderConsideration)*100;
        print("Percentage contibution of High Positive: "+PercentRegion4);
        print("Percentage contibution of Positive: "+PercentRegion3);
        print("Percentage contibution of Low Positive: "+PercentRegion2);
        print("Percentage contibution of Negative: "+PercentRegion1);
                Score=Score+(PercentRegion4/100)*4+(PercentRegion3/100)*3+(PercentRegion2/100)*2+(PercentRegion1/10
0)*1;
                print("The score is: "+Score);
```

This code measures the intensity of each pixel in the image generate a histogram of the intensity distribution. Then the intensities are binned to 5 different regions and the percentage of each of the 5 bins were calculated. The most brown, or the pixel of lowest intensity was binned to region 1 and given a score of 4. Like wise, less brown and brighter pixel was given lower score and regions of higher order. Region 5 contains the white back which was subtract from the total pixels. The process returns a score and quantify the DAB blue stain within the region of interest.

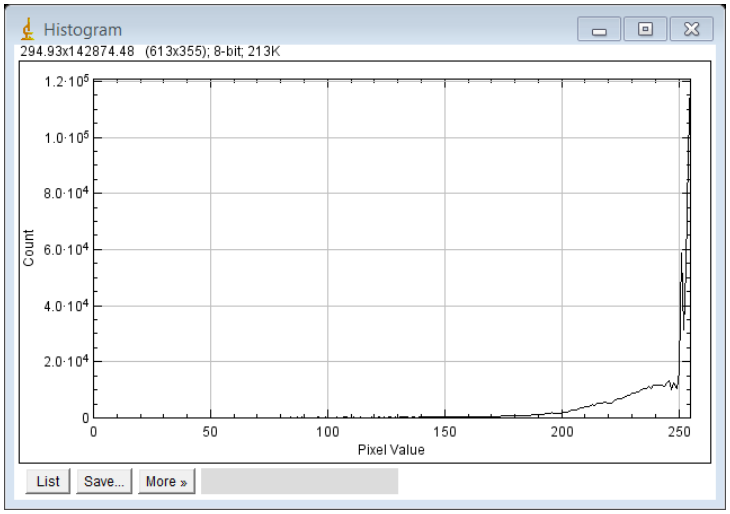
Histogram
294.93x142874.48 (613x355); 8-bit; 213K
1.2·10^5
1.0·10^5
8.0·10^4
6.0·10^4
4.0·10^4
2.0·10^4
0
Count
0
50
100
150
200
250
Pixel Value
List
Save...
More »

2. ImageJ Macro to Quantify Alcian Blue Stain

A macro in ImageJ was used to split images of Alcian blue stain from the counterstain of nuclear fast red and return predefined 8-bit images of only Alcian blue. The threshold was determined from Alcian blue stain of native patella osteochondral interface.

For measurements, an Alcian blue image was loaded in ImageJ.

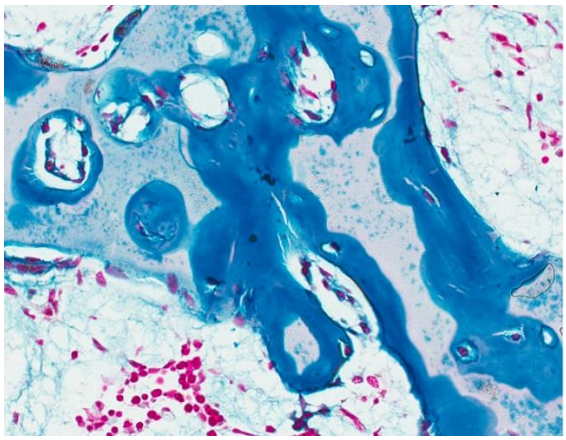

Then, the following code will split the channels:

```
run("Colour Deconvolution", "vectors=[User values] [r1]=16.456932 [g1]=255 [b1]=43.27766 [r2]=255 [g2]=50.3366 [b2]=20.996815 [r3]=3.9401577 [g3]=2.3609867 [b3]=2.593382");
```

This code returns three images of only nuclear fast red, Alcian blue and residue.

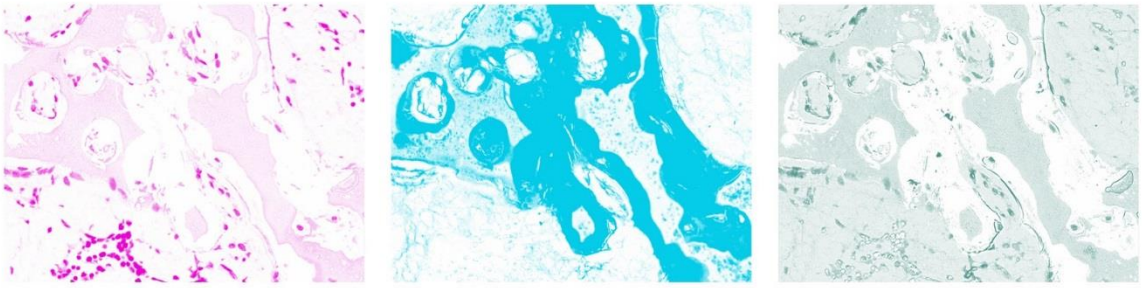

Nuclear fast red (Channel 1) Alcian blue (Channel 2) Residual image (Channel 3)

After that, channel 2 which only contains Alcian blue stain in 8 bit was analyze by a macro in the plugin of IHC profiler using the following code:

```
bins = 256;
 maxCount = 0;
 histMin = 0;
 histMax = 0;
 if (histMax>0)
        getHistogram(values, counts, bins, histMin, histMax);
```

```
else
        getHistogram(values, counts, bins);
is8bits = bitDepth()==8 || bitDepth()==24;
Plot.create("Histogram", "Pixel Value", "Count", values, counts);
if (maxCount>0)
        Plot.setLimits(0, 256, 0, maxCount);
n = 0;
sum = 0;
min = 9999999;
max = -9999999;
Region2=0;
Region3=0;
Region4=0;
Region1=0;
Region0=0;
TotalPixel=0;
PercentRegion1=0;
PercentRegion2=0;
PercentRegion4=0;
PercentRegion3=0;
PercentRegion0=0;
Score=0;
PixelUnderConsideration=0;
for (i=0; i<bins; i++)
        {
    count = counts[i];
    if (count>0)
                {
         n += count;
         sum += count*i;
         if (i<min) min = i;
         if (i>max) max = i;
        }
        }
var x=0.025, y=0.1; // global variables
print("Pixel Count: "+n);
if (is8bits)
        {
```

```
                for (i=0; i<bins; i++)
                        {
                    if (i>=0 && i<61)
                            Region4=Region4+counts[i];
                        if (i>60 && i<121)
                    Region3=Region3+counts[i];
                        if (i>120 && i<181)
                    Region2=Region2+counts[i];
                        if (i>180 && i<236)
                    Region1=Region1+counts[i];
                if (i>235 && i<=256)
                    Region0=Region0+counts[i];
                        }
                }
        function draw(text)
                {
                 Plot.addText(text, x, y);
            y += 0.08;
                }
        TotalPixel=TotalPixel+Region1+Region2+Region3+Region4+Region0;
        PixelUnderConsideration=TotalPixel-Region0;
        PercentRegion3=(Region3/PixelUnderConsideration)*100;
        PercentRegion2=(Region2/PixelUnderConsideration)*100;
        PercentRegion1=(Region1/PixelUnderConsideration)*100;
        PercentRegion4=(Region4/PixelUnderConsideration)*100;
        print("Percentage contibution of High Positive: "+PercentRegion4);
        print("Percentage contibution of Positive: "+PercentRegion3);
        print("Percentage contibution of Low Positive: "+PercentRegion2);
        print("Percentage contibution of Negative: "+PercentRegion1);
                Score=Score+(PercentRegion4/100)*4+(PercentRegion3/100)*3+(PercentRegion2/100)*2+(PercentRegion1/10
0)*1;
                print("The score is: "+Score);
```

This code measures the intensity of each pixel in the image generate a histogram of the intensity distribution. Then the intensities are binned to 5 different regions and the percentage of each of the 5 bins were calculated. The most blue, or the pixel of lowest intensity was binned to region 1 and given a score of 4. Like wise, less blue and brighter pixel was given lower score and regions of higher order. Region 5 contains the white back which was subtract from the total pixels. The process returns a score and quantify the Alcian blue stain within the region of interest.

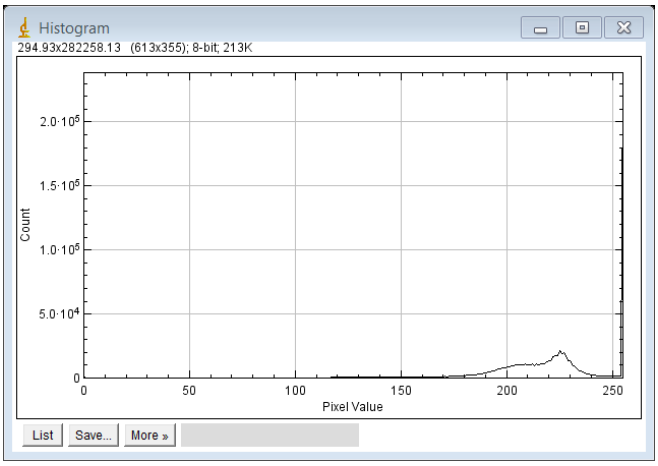
Histogram
294.93x282258.13 (613x355); 8-bit; 213K
2.0·10^5
1.5·10^5
1.0·10^5
5.0·10^4
0
Count
0
50
100
150
200
250
Pixel Value
List
Save...
More »

Appendix 4: Preparation of SEM Samples

Samples were fixed in 2% glutaraldehyde in 0.05M cacodylate buffer (pH=7.4) for 2 hours at 4°C, followed by a wash in 0.05M cacodylate buffer for 10 minutes at room temperature. Then, the samples were treated with 1% osmium tetroxide in the cacodylate buffer for 1 hour at room temperature and rinsed 3 times with in cacodylate buffer for 10 minutes. The fixed samples were dehydrated in serial dilution of ethanol and stored in 100% ethanol for 48 hours. These samples were further dried in a critical point dryer and sputter-coated with Au-Pd.